IS-T 1754

SPECTRAL HOLE BURNING STUDIES OF PHOTOSYSTEM II

by

Chang, Hai-Chou

MS Thesis submitted to Iowa State University

Ames Laboratory, U.S. DOE
Iowa State University
Ames, Iowa 50011

Date Transmitted: September 26, 1995

PREPARED FOR THE U.S. DEPARTMENT OF ENERGY
UNDER CONTRACT NO. W-7405-Eng-82.

DISCLAIMER

Spectral hole burning studies of Photosystem II

Hai-Chou Chang

Major Professors: Drs. Gerald J. Small/ Walter S. Struve
Iowa State University

Low temperature absorption and hole burning spectroscopies were applied to the D1-D2-cyt b_{559}, and the CP47 and CP43 antenna protein complexes of Photosystem II from higher plants. Low temperature transient and persistent hole-burning data and theoretical calculations on the kinetics and temperature dependence of the P680 hole profile are presented and provide convincing support for the linker model. Implicit in the linker model is that the 684-nm-absorbing Chl *a* serve to shuttle energy from the proximal antenna complex to reaction center. The stoichiometry of isolated Photosystem II Reaction Center (PSII RC) in several different preparations is also discussed. The additional Chl *a* are due to 684-nm-absorbing Chl *a*, some contamination by the CP47 complex, and non-native Chl *a* absorbing near 670 nm. In the CP47 protein complex, attention is focused on the lower energy chlorophyll *a* Q_y-states. On the basis of the analysis of the hole and static fluorescence spectra at 4.2 K, the lowest energy state of CP47 was found to be at 690 nm. The 690 nm and 687 nm states are excitonically correlated and correspond to an excitonically coupled dimer. High pressure hole-burning studies of PSII RC revealed for the first time a strong pressure effect on the primary electron transfer dynamics. The 4.2 K lifetime of $P680^*$, the primary donor state, increases from 2.0 ps to 7.0 ps as pressure increases from 0.1 to 267 MPa. Importantly, this effect is irreversible (plastic) while the pressure induced effect on the low temperature absorption and non-line narrowed P680 hole spectra are reversible (elastic). Nonadiabatic rate

expressions, which take into account the distribution of energy gap values, are used to estimate the linear pressure shift of the acceptor state energy for both the superexchange and two-step mechanisms for primary charge separation. It was found that the pressure dependence could be explained with a linear pressure shift of ≈ 1 cm^{-1}/MPa in magnitude for the acceptor state. The results point to the marriage of hole burning and high pressures as having considerable potential for the study of primary transport dynamics in reaction centers and antenna complexes.

TABLE OF CONTENTS

CHAPTER 1 GENERAL REMARKS ON PHOTOSYNTHESIS

1.1 Dissertation Organization

This dissertation contains the candidate's original work on spectral hole burning of Photosystem II. General introduction is divided into three chapters (chapters 1-3). Photosynthesis, spectral hole burning spectroscopies, and theoretical background are described in chapter 1, 2, and 3, respectively. Chapter 4 contains one published paper which report hole burning experiments performed on the CP47 complex. Chapters 5, 6 and 7 are published papers which report experiments performed on the Photosystem II reaction center. Each of these published works contains a description of the experimental apparatus as it was used for the specific experiment. Additional results of the CP43 complex and Photosystem II reaction center are described in the appendix. The references for each chapter are found at the end of that chapter.

1.2 Introduction

Most of the energy which is available on earth comes from photosynthesis. Every year 3×10^{21} joules of energy are stored by photosynthesis [1]. Therefore, as our reserves of energy diminish, it becomes important to understand how photosynthesis works. The whole process of photosynthesis can be resolved into numerous reaction steps [1-3]. An overall equation of the process that occurs is [1-3]

$$nCO_2 + 2nH_2A + h\upsilon \rightarrow n(CH_2O) + 2nA + nH_2O \qquad (1)$$

where (CH_2O) represents part of a carbohydrate molecule and H_2A is the oxidizable substrate, such as H_2O or H_2S. Photosynthesis can be regarded as a process of converting radiant energy of the sun into chemical energy.

Photosynthesis in green plants takes place inside of the chloroplasts. The apparatus used by plants to perform photosynthesis is both complex and highly efficient. As shown in Figure 1, three different membranes (outer, inner, and thylakoid membranes) divide the chloroplast into three separate spaces (intermembrane, stroma, and thylakoid spaces or lumen) [1-3]. The stroma that surrounds the thylakoid membrane contains the enzymes responsible for the actual fixation of CO_2 and the synthesis of carbohydrates. The thylakoid membranes are very important to the primary steps of photosynthesis. The photosynthetic proteins, such as the light-harvesting proteins, and reaction centers are buried inside the thylakoid membranes [1-3]. The pigment molecules are specifically bound to proteins which determine the positions, environments, orientations and spacings of the pigment molecules. Chlorophyll *a* and *b* are the primary photoreceptors of green plants. The absorption spectra of chlorophyll *a* (Chl *a*) and chlorophyll *b* (Chl *b*) are different [1-3]. Thus, coexistence of these two kinds of chlorophyll is important to the absorption of a wide range of solar wavelengths. The incorporation of different pigments (e.g., Chl *a*, Chl *b*, and carotenoids), absorbing at different wavelengths, allows the photosynthetic unit to use a greater portion of the solar spectrum.

Functionally, pigmented proteins are divided into two classes: antenna and reaction center complexes (RC). The initial event in photosynthesis is the capture of light by antenna. Light absorbed by antenna pigments leads to singlet excitons. The funneling of these excitons to the reaction centers induces electron transfer. Finally the energy of electron flow is stored in chemical forms.

Antenna only absorb light and cannot transform the energy of light into chemical energy. The antenna systems are generally characterized by different absorption maxima and form "ladder " systems for heterogeneous and directed excited energy transfer (EET)

[4,5]. Antenna chromophores nearer to the reaction center absorb at longer wavelengths, leading to an energy funneling effect. This downhill transfer has been shown to increase trapping rates by as much as a factor of ten [5].

Photosynthesis by oxygen-evolving organisms is comprised of two photosystem mechanisms: Photosystem I (PSI) and Photosystem II (PSII). The excitation energy is

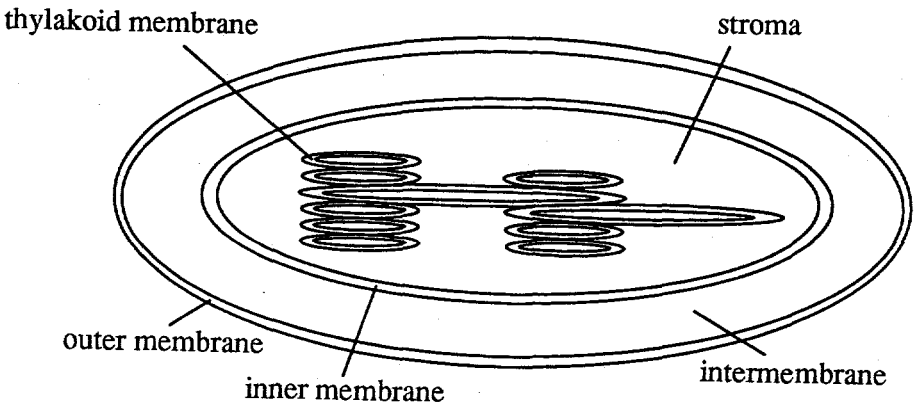

Figure 1. Diagram of chloroplast structure. Chloroplasts have three different membranes (outer, inner, and thylakoid membranes) and three separate space (intermembrane, stroma, and lumen). The thylakoid membranes contain the energy-transducing machinery.

transferred to the reaction centers: P680 in PSII, and P700 in PSI. Photosystem I leads to the formation of NADPH. Photosystem II generates a strong oxidant $P680^+$ which extracts electrons from water and leads to the formation of O_2.

The mechanism of electron transport of green plants is called the Z-scheme (Figure 2). The primary charge separation of Photosystem II leads to the formation of $P680^+$ and $Pheo^-$. $P680^+$ is reduced via various steps (indicated as S) by an electron which is

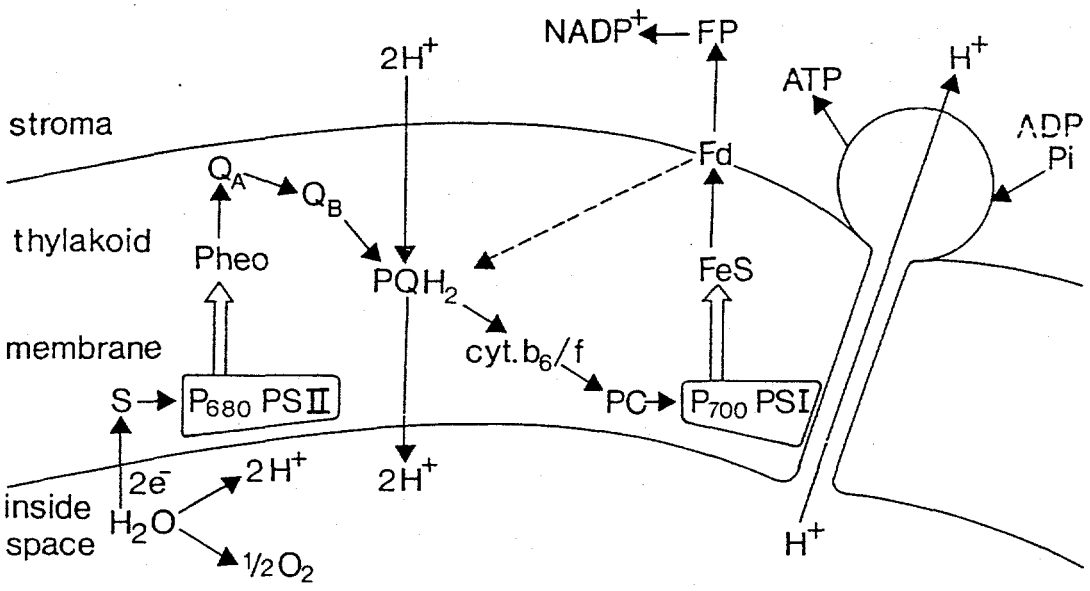

Figure 2. Pathway of electron and proton flow in photosynthesis of green plants.

ultimately derived from water [1-3]. From $Pheo^-$, the electron is transported to the first quinone Q_A and then to the secondary quinone Q_B. Q_B accumulates two electrons and becomes protonated with two protons from the stroma and exchanges with the plastoquinone pool (PQH_2). From PQH_2, electrons are transferred to the cytochrome b_6/ cytochrome f (cyt b_6/f) complex and two protons are liberated into the internal lumen of the thylakoid. Plastocyanin (PC) transfers a electron to $P700^+$ to fill the electron hole produced by the primary separation of Photosystem I. The electron is transferred to FeS centers. Eventually the high energy electron flow leads to the formation of NADPH and ATP.

1.3 Photosystem II And The Similarity To Bacteria

As shown in Figure 3, the main portion of the light-harvesting antenna of Photosystem II is made up of several chlorophyll *a*/*b*-proteins, mainly LHCII. LHCII is the most abundant pigment protein of the thylakoid membrane. Based on the analysis of the crystal structure of LHCII complex, a trimeric structure of triangular shape has been resolved and also believed to be the native form [6,7]. All chlorophylls are arranged in two levels near the upper and lower surfaces of the thylakoid membrane [6,7]. The shortest center-to-center distances between Chls were estimated to be less than 15 Å [6,7]. The densely-packed structure of LHCII demonstrates that excitonic interactions can play an important role in antenna systems. LHCII is connected with the reaction center complex via other chlorophyll proteins referred to as CP24, CP26, and CP29. There are also two more major chlorophyll *a* proteins (CP47 and CP43) which are more tightly associated with the reaction center. CP47 and CP43 are called inner antenna which serve as the intermediary between LHCII and Photosystem II reaction center. Additional discussion of CP47 and CP43 can be found in Chapter 5 and the appendix A, respectively.

Consequently the light energy captured by the antenna is transferred to the primary electron donor P680 of Phtosystem II reaction center where the electron transport starts.

It is particularly interesting to ask whether or not the structures and functions of Photosystem II RC are similar to those of bacterial RCs. As resolved by an X-ray

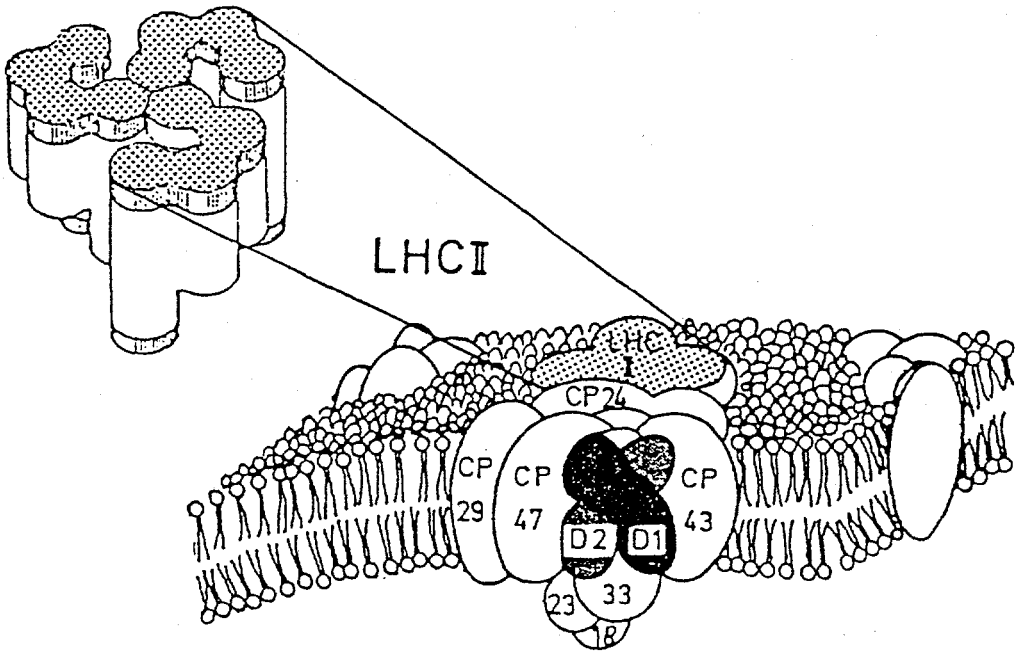

Figure 3. Simplified scheme of the incorporation of antenna-pigment protein complexes into the thylakoid membrane of green plants. The light-harvesting complex II is explicitely shown. CP= chlorophyll-protein complexes, numbers refer to the approximate molecular weight of the polypeptides. The cytochrome complex and PSI are not explicitely shown in the membrane section.

crystallograph [8,9] (see Figure 4), the purple bacterial reaction center from *Rps. viridis* carries four BChl, two BPheo, and two menaquinone (Q_A, Q_B). Two closely-coupled BChl molecules (P_L, P_M) comprise a "special pair" that functions as the primary electron donor. One BPheo (H_L) is the proximal acceptor, receiving an electron from a special pair in 3 ps [14]. The electron moves in 200 ps to a quinone acceptor (Q_A) and subsequently, in 60 μs, to a secondary quinone (Q_B). These pigments are organized in two almost identical branches by the L and M proteins. With the availability of the X-ray structure of *Rps. viridis* [8,9] significant homologies between the amino acid sequences of the L and M subunits of the bacterial RC and D1 and D2 proteins of PSII were realized [10]. This discovery led several groups [9,11,12] to predict that the D1 and D2 proteins were homologous to the L and M subunits in both structure and function.

In 1987 Nanba and Satoh announced the method which can extract the reaction center of PSII from green plants [13]. As predicted, the isolated PSII reaction center contained D1, D2, and cyt b_{559}. The homologies of the amino acid sequences between bacterial and PSII reaction centers suggest that the structure of both may be similar, although there is no crystallographic proof yet. Photosystem II RC, i.e., D1-D2-cytb_{559} complex, contains 4-6 Chl *a*, 2 Pheo *a*, 1 or 2 β-carotenes, 1 cytochrome b_{559} and no plastoquinones (see chapter 5). The pigment cofactor composition of D1-D2-cytb_{559} complex also resembles that of bacterial RCs. As a consequence, it was suggested that P680 is most likely a dimer [14]. Certain optical properties suggest a dimeric structure for P680 as well [14-17]. For example, spectral hole burning studies of the PSII RC yielded data which strongly indicate that P680 is a special pair with a dimer splitting of only 300 cm^{-1} [16,17]. The Q_y transition moments of two monomers are nearly anti-parallel. This geometry results in nearly all transition probability being found in one of the two exciton

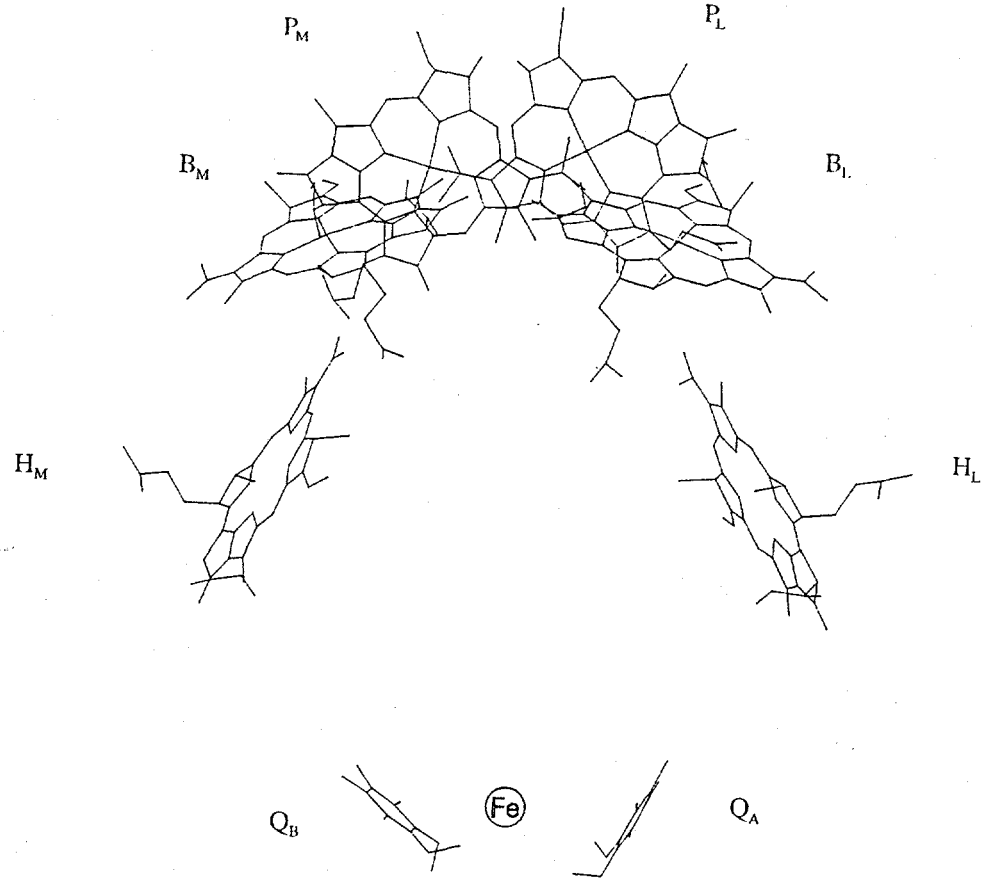

Figure 4. Structure of the reaction center of purple bacteria. Four bacteriochlorophylls (P_L, P_M, B_L, B_M), two bacteriopheophytin (H_L, H_M) and two menaquinone (Q_A, Q_B) are shown. The molecules are arranged in two branches, L and M forming an approximate C_2-symmetry.

bands. On the basis of the 300 cm^{-1} splitting, Kwa et al. [17] deduce that the separation (Mg•••Mg) between the monomers of P680 is ~11Å. Therefore, P680 is a relatively weak coupled special pair, but may be disguised as a monomer by the geometry of two monomers.

As indicated in Figure 5, the kinetics scheme of PSII RC shows the similarity with that of bacterial RC. The primary charge separation in PSII ($P680^* + Pheo \rightarrow P680^+ + Pheo^-$) takes place in a few picoseconds in the isolated D1-D2-cyt b_{559} complex (3.0 ps at 277K [18] and 1.9 ps at 4.2K [16], respectively). The rate of the process of the electron transfer from $Pheo^-$ to Q_A was determined from PSII membrane fragment or PSII core complex instead of D1-D2-cyt b_{559} complex which does not have Q_A. The rate of Q_A^- formation exhibits a half-rise time of about 300 ps [19,20]. The reduction kinetics of Q_A in PSII are slightly slower than those of the corresponding reaction in bacteria (200 ps). Q_A^- transfers the electron to the secondary quinone Q_B, which is a two-electron carrier. The rate of electron transfer from Q_A^- depends on the reduced state of the secondary quinone. A value of 100-200 μs is observed for the first reduction, but is increased to 300-500 μs for the second reduction [19,20].

1.4 Superexchange Or Two-Step

The basic arguments involved in the understanding of the bacterial reaction center are not settled even though the crystal structure has been solved. One of the major reasons is that the information required for excited-state dynamics can not be obtained directly from the X-ray structure in the ground state. Whether or not $P^+B_L^-$ serves as a real or virtual state in the primary charge separation process is one of the long-standing questions [21,22]. Three mechanisms have been proposed: (i) one-step superexchange mechanisms in which $P^+B_L^-H_L$ is simply a virtual state and $P^+B_LH_L^-$ serves as the acceptor state.

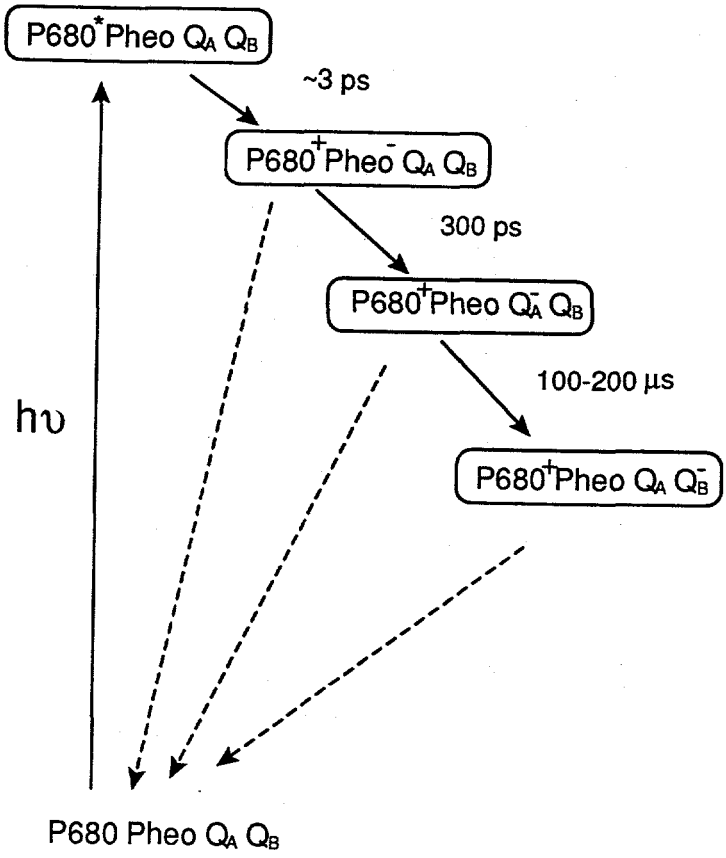

Figure 5. Reaction scheme of primary processes in the reaction center of Photosystem II at room temperature. P680, Pheo, Q_A, and Q_B represent the primary donor, pheophytin, first and secondary quinone, respectively. The rate of the second reduction of Q_B (300-500 µs) is not shown.

(ii) two-step mechanism; here $P^+B_L^-H_L$ is a real state and serves as the acceptor state. The electron is subsequently transfered to the second state, i.e., $P^+B_LH_L^-$. (iii) the parallel sequential-superexchange mechanism; this mechanism includes both superexchange and two-step mechanisms as limiting cases.

In order to illustrate the major differences between the superexchange and the two-step mechanisms, we consider the general multilevel multimode system of the excited states [23,24]. The Hamiltonian can be written as

$$H = \sum_{i=1}^{N} \varepsilon_i |i\rangle\langle i| + \sum_{i<j}{}' J_{ij} |i\rangle\langle j| + \sum_{n=1}^{M} \omega_n b_n^+ b_n + \sum_{ij} \sum_{n}^{M} \theta_{ij}^n |i\rangle\langle j| (b_n + b_n^+) \qquad (2)$$

where N is the number of excited states involved and M is the number of vibrational modes. $|i\rangle$ is the excited state with electronic energy ε_{ii}. J_{ij} is the electronic coupling element between states $|i\rangle$ and $|j\rangle$ and ω_n is the vibrational frequency of mode n. θ_{ij}^n corresponds to vibronic coupling parameter. Assume a dipole allowed excited state D to interact with a dipole forbidden excited state A. Note that, in the case of bacterial RC, D is the lowest energy state (P_-) of the special pair and A corresponds to $P^+B_L^-$. Then

$$\langle 0|\mu|D\rangle \neq 0 \qquad (3)$$

and

$$\langle 0|\mu|A\rangle = 0 \qquad (4)$$

where $|0\rangle$ represents the ground electronic state. Eq.2 is rewritten as

$$H = \sum_{i=D,A} \varepsilon_i |i\rangle\langle i| + \sum_{i,j=D,A}{}' J_{ij} |i\rangle\langle j| + \omega b^+ b + \sum_{i,j=D,A} \theta_{ij} |i\rangle\langle j| (b^+ + b) \qquad (5)$$

For simplicity, we consider only one vibrational mode with frequency ω and define $|\Delta E| = |\varepsilon_D - \varepsilon_A|$. The calculations of Friesner et al. [23] reveal how, for a fixed $|\Delta E|$ and J, the extent to which the $|D\rangle$ state steals S from the $|A\rangle$ state increases in passing from $\theta/\omega < 1$ to $\theta/\omega > 1$ where the adiabatic limit is in effect. That is, Huang-Rhys factor of P_- state ($|D\rangle$ state) is not affected by $P^+B_L^-$ ($|A\rangle$ state) in the weak coupling limit.

It is known from the data of spectral hole burning that a zero-order P^* state, with weak electron-phonon coupling, receives the Huang-Rhys factor (S) from a charge transfer state through the coupling (or electronic state mixing) between these two states. (The key observation is that the electron-phonon coupling for P_+ is weak, but strong for P_- of *Rb. sphaeroides* RC [24].) To explain this observation, one must consider the coupling between the lowest energy excited electronic state (P_-) of the special pair with weak electron-phonon coupling and a nearby external charge transfer state ($P^+B_L^-$) with strong electron-phonon coupling (see Small [24] for detail). In order to explain the effect of the "stealing" of S from the dark charge transfer state, the case of a strong coupling limit needs to be addressed.

The strong coupling between P_- and $P^+B_L^-$ results in an adiabatic energy surface associated with two wells, as indicated in Figure 1 of Chapter 3. These two wells originate from the nonadiabatic P_- and $P^+B_L^-$ surfaces, respectively. Therefore, the question of whether or not $P^+B_L^-$ serves as a real or virtual state in the primary charge separation process becomes irrelevant in the strong coupling limit.

References

1. Hall,D.O.; Rao,K.K. in *Photosynthesis*; Cambridge Press: Cambridge, 1994
2. Zubay,G. in *Biochemistry*; Addison-Wesley: Reading, 1983
3. Stryer,L. in *Biochemistry*; Freeman: New York, 1988

4. Zuber,H.; Brunisholz,R.; Sidler,W. in *Photosynthesis*; Amesz,J., Ed.; Elsevier: The Netherland, 1987

5. Borisov,A.Y.; Fetisova,Z.G. *Mol. Biol.* 1971, 5, 509

6. Kühlbrandt,W.; Wang,D.N. *Nature* 1991, 350, 130

7. Kühlbrandt,W.; Wang,D.N.; Fujiyoshi,Y. *Nature* 1994, 367, 614

8. Deisenhofer,J.; Epp,O.; Miki,K.; Huber,R.; Michel,H. *J. Mol. Biol.* 1984, 180, 385

9. Deisenhofer,J.; Epp,O.; Miki,K.; Huber,R.; Michel,H. *Nature* 1985, 318, 618

10. Rochaix,J.D.; Dron,M.; Rahire,M.; Malnoe,P. *Plant Mol. Biol.* 1984, 3, 363

11. Cramer,W.A.; Widger,W.R.; Herrmann,R.G.; Trebst,A. *Trends Biochem. Sci.* 1985, 10, 125

12. Kyle,D.J. *Photochem. Photobiol.* 1985, 41, 107

13. Nanba,O.; Satoh,K. *Proc. Natl. Acad. Sci. USA* 1987, 84, 109

14. Seibert,M. in *The Photosynthetic Reaction Center*, Vol.I; Deisenhofer,J., Norris,J., Eds.; Academic Press: New York, 1993, p.319

15. Braun,P.; Greenberg,B.M.; Scherz,A. *Biochem.* 1990, 29, 10376

16. Chang,H.-C.; Jankowiak,R.; Reddy,N.R.S.; Yocum,C.F.; Picorel,R.; Seibert,M.; Small,G.J. *J. Phys. Chem.* 1994, 98, 7725

17. Kwa,S.L.S.; Eijckelhoff,C.; van Grondelle,R.; Dekker,J.P. *J. Phys. Chem.* 1994, 98, 7702

18. Wasielewski,M.R.; Johnson,D.G.; Seibert,M.; Govindjee *Proc. Natl. Acad. Sci.* 1989, 86, 524

19. Evans,M.C.W.; Nugent,J.H.A. in *The Photosynthetic Reaction Center*, Vol.I, Deisenhofer,J., Norris,J., Eds.; Academic Press: New York, 1993, p.391

20. Renger,G. in *Topics in Photosynthesis*, Vol.11; Barber,J., Ed.; Elsevier: The Netherland, 1992, p.45

21. Bixon,M.; Jortner,J.; Michel-Beyerle,M.E. in *The Photosynthetic Bacterial Reaction Center II*; Breton,J., Vermeglio,A., Eds.; NATO-ASI series A, Vol.237; Plenum Press: New York, 1992, p.291

22. Bixon,M.; Jortner,J.; Michel-Beyerle,M.E. *Chem. Phys.* (in press) and references therein.

23. Lathrop,E.J.P.; Friesner,R.A. *J. Phys. Chem.* 1994, 98, 3050

24. Small,G.J. *Chem. Phys.* in press

CHAPTER 2 SPECTRAL HOLE BURNING SPECTROSCOPIES

2.1 Introduction

Fundamentally amorphous systems are not in thermodynamic equilibrium. Various local structures make dominant contributions to the properties of amorphous systems, and, as indicated in Figure 1, the absorbing centers are surrounded by different local environments [1]. The distribution of these local environments results in inhomogeneous broadening (Γ_{inh}). In order to observe a homogeneous line width and obtain useful information about the dynamics of an amorphous system, spectral hole burning can be effective. It removes the inhomogeneous broadening. Proteins, like glass, possess many conformational substates which may transform from one state to another state by virtue of thermal energies [2]. As the temperature goes down to the temperature of liquid helium, the transformations among the substates are frozen and the distribution of these substates results in inhomogeneity. To put proteins in perspective, the intrinsic glass-like character of proteins needs to be adequately addressed. Therefore, spectral hole burning serves as a useful tool in the studies of proteins [3-5].

The invention of the narrowband laser provided a suitable excitation source for spectral hole burning. This provided an improvement in the resolution of the optical spectra by 2-3 orders of magnitude [6]. Typically these holes, burned at very low temperatures, are narrow and sensitive to the microscopic environment. A zero-phonon hole is the one with no net change in the number of phonons which accompany the electronic transition. The width of the zero-phonon line (ZPL) is mainly determined by homogeneous broadening which originates with the effective decay time of excited molecules. The effective decay time is described [7] as

$$\frac{2}{T_2} = \frac{1}{T_1} + \frac{2}{T_2^*} \tag{1}$$

where T_1 is the lifetime of the excited state and T_2^* is the pure dephasing time of the molecules. Eq.1 is not symmetric in T_1 and T_2^*, because the scattering processes with characteristic time T_2^* can occur in both the ground and excited state [1]. That is why the

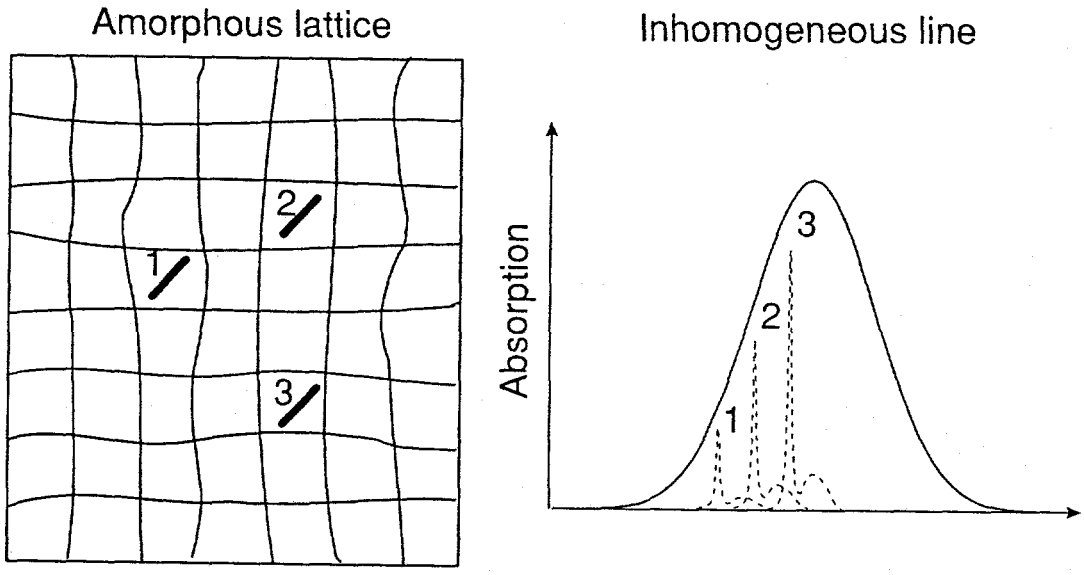

Figure 1. Schematic view of the optical absorption of three identical guest molecules in an amorphous host. In contrast to the situation in a crystalline lattice, the lines appear at different transition frequencies. The broad sidebands represent the phonon spectra of molecules 1, 2, and 3, respectively.

term of T_2^* owns a factor of two. Glass or proteins provide a high density of very low-frequency lattice states (due to the presence of two-level systems) which cause broadening via dephasing [6]. Due to the disappearance of thermal-excited lattice modes, the dephasing time is increased with decreasing temperature. As the temperature approaches zero, the zero-phonon hole width approaches its limiting value determined by T_1. Eq.1 is rewritten as

$$\frac{2}{T_2} = \frac{1}{T_1} \quad \text{or} \quad T_2 = 2T_1 \tag{2}$$

The absorption spectrum after a burn for time τ at a frequency of ω_B in the low termperature limit is written as (see section 3.3)

$$A_\tau(\Omega) = \int d\upsilon N_\tau(\upsilon - \upsilon_m) L(\Omega - \upsilon)$$

$$= \sum_{p=0}^{\infty} \frac{e^{-S} S^P}{P!} \int d\upsilon N_0(\upsilon - \upsilon_m) \exp[-\sigma I \phi \tau L(\omega_B - \upsilon)]$$

$$\times l_p(\Omega - \upsilon - p\omega_m) \tag{3}$$

Consider the case of the short burn time limit [8] which we are intersted in. Then

$$\exp[-\sigma I \phi \tau L(\omega_B - \upsilon)] = 1 - \sigma I \phi \tau L(\omega_B - \upsilon) \tag{4}$$

Substitution Eq.4 into Eq.3 leads to

$$A_\tau(\Omega) = \sum_{p=0}^{\infty} \frac{e^{-S} S^p}{p!} \int d\upsilon N_0(\upsilon - \upsilon_m)(1 - \sigma I \phi \tau L(\omega_B - \upsilon))$$

$$\times l_p(\Omega - \upsilon - p\omega_m) \tag{5}$$

The hole profile is given by

$$A_\tau(\Omega) - A_0(\Omega) = -\sum_{p=0}^{\infty} \frac{e^{-S} S^p}{p!} \int d\upsilon N_0(\upsilon - \upsilon_m)$$

$$\times \sigma I \phi \tau L(\omega_B - \upsilon) l_p(\Omega - \upsilon - p\omega_B) \qquad (6)$$

Thus the hole profile is the convolution of two Lorentzians. Assuming $\Delta\upsilon_h$ is the full width at half-maximum of the Lorentzians, we have

$$\Gamma_{hole} = 2\Delta\upsilon_h \qquad (7)$$

where Γ_{hole} is the full width at half-maximum of the hole measured. The uncertainty principle leads to

$$\Delta\upsilon_h = \frac{1}{2\pi T_1} \qquad (8)$$

By substituting Eq.2 and Eq.8 into Eq.7, the relationship between measured hole-width and total dephasing time is written as

$$\Gamma_{hole} = \frac{2}{\pi T_2} \qquad (9)$$

2.2 NPHB, PHB vs Bottleneck HB: Mechanistic Aspects

Three basic hole-burning mechanisms can be described [3]. These are referred to as photochemical hole burning (PHB), nonphotochemical hole burning (NPHB), and transient hole burning. Photochemical hole burning [1] means the absorbing center (the guest) is involved in some internal change, such as tautomerization, bond-breaking,

isomerization, and so on. If the absorbing center is photoreactive, selective photobleaching of absorption spectrum can be engineered. What is required for PHB is the photoreactivity of the absorbing chromophore. Therefore, PHB can be observed for both amorphous and crystalline hosts. Photochemical hole burning was first observed [9] for free base phthalocyanine in n-octane where the PHB is caused by an intramolecular hydrogen tautomerization. In PHB the antihole is usually not near the zero-phonon hole as shown in Figure 2. The antihole is usually much broader than its parent hole because of the inhomogeneous broadening of the zero phonon lines of the photoproducts.

In the case of nonphotochemical hole burning, photoreactivity of the absorbing centers is not required. Nonphotochemical processes result from the change of the environment (the host) around the absorbing center. As indicated in Figure 2, absorption positions of the products (antihole) for nonphotochemical processes are not moved very far from the original absorption position. Since the host configurations need to be changed in the case of NPHB, NPHB has only been observed with glasses and polymers, with a few exceptions [8]. Nonphotochemical hole burning was first observed [10] for perylene and for 9-aminoacridine in the ethanol glass. The nonphotochemical holes often irreversibly disappear after increasing the temperature. In 1972, Anderson et al. [11] and, independently, Phillips [12] proposed that in any glass system there should be a certain number of atoms or groups of atoms which may occupy, with nearly equal probability, two equilibrium positions separated by an energy barrier, the so-called two-level system (TLS) (see Figure 3). At very low temperatures, atoms or groups of atoms cannot be thermally activated over the barrier, but can tunnel through it. As indicated in Figure 3, the excited molecules are produced by the excitation light (ω_B). At the burn temperature, relaxation between the minima of ground state TLS_α is slow on the time scale of the experiment,

while it is competitive with the excited state lifetime at TLSβ (β denotes the impurity excited state). The degree of competiveness determines the hole burning efficiency.

In 1978 the two-level system (TLS) model, based on the coupling of the electronic transition to the glass TLS_{ext}, was utilized for the NPHB mechanism [13]. Extrinsic TLSs (TLS_{ext}) are suggested to be strongly associated with the absorbing center and are

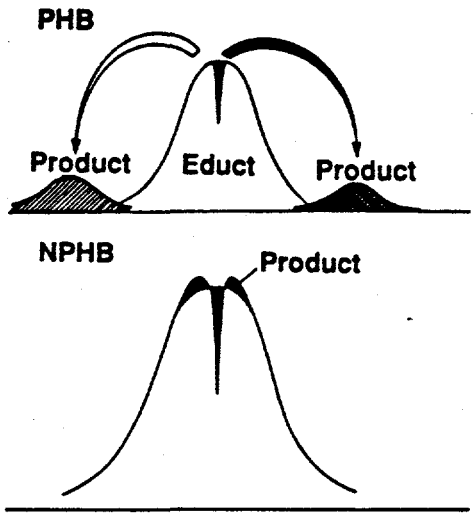

Figure 2. Spectral distribution of the photoproducts after photochemical (PHB) and nonphotochemical (NPHB) hole burning.

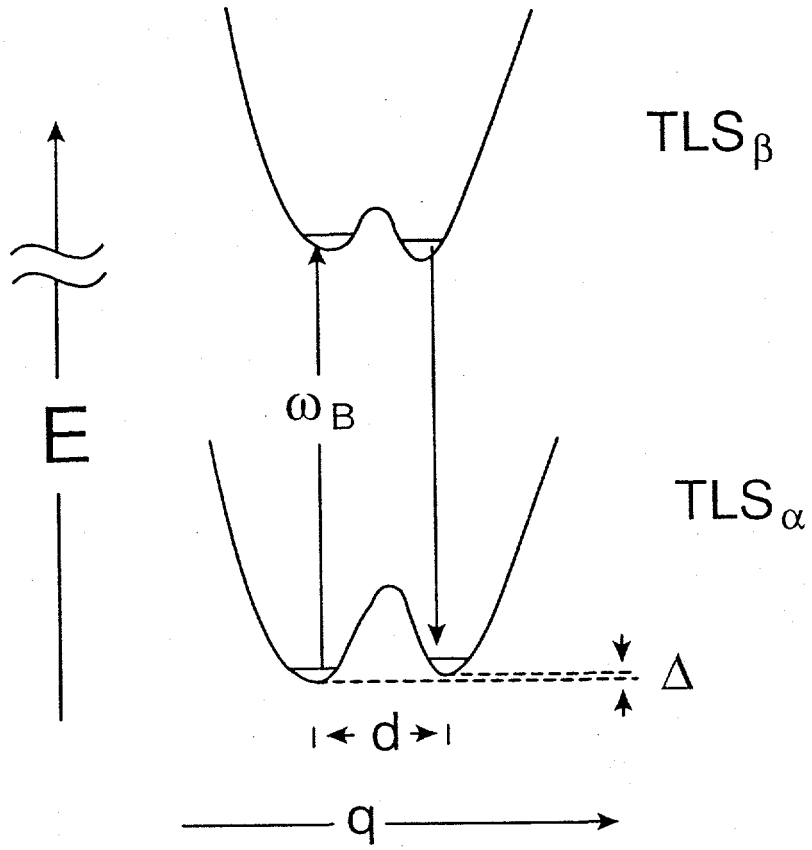

Figure 3. The two-level system (TLS) model for nonphotochemical hole burning. The subscripts α and β label the TLS that interact with the impurity in its ground and excited electronic states. Asymmetries, displacements, intermolecular coordinates are labeled as Δ, d, and q, respectively.

responsible for the initiation of hole burning. NPHB occurs primarily in amorphous (glassy) matrices due to a rearrangement of the host enviroment , triggered by the electron-TLS_{ex} coupling. The rate-determining step for hole formation is phonon-assisted tunneling of TLS_{ext}. The intrinsic bistable configuration of the host itself is denoted by TLS_{int}. The intrinsic TLSs (TLS_{int}) was proposed to cause optical dephasing [8,13]. The mechanistic model for persistent NPHB was further developed by Shu et al. [14]. NPHB is triggered by electronic excitation and results in an increase in the free volume of the probe. An increase in the free volume for the probe in its inner shell of host molecules successfully explained the blue-shift of the antihole since $^1\pi\pi^*$ states typically undergo a red-shift in going from the gas to the condensed phase. From the above we know that NPHB is the result of phonon-assisted tunneling of TLSs and provides a physical observance of TLS relaxation.

In NPHB only two electronic states of the quest molecules are involved (the ground and excited states). Population bottleneck hole burning utilizes a third, long-lived state to store the population depleted from the ground state [3,4]. The triplet state is usually the suitable candidate to serve as a population reservoir. In transient hole burning of bacterial reaction center, however, the analogous state is a product of the charge separation state of the primary electron donor, P^*. Although photoexcitation of P results in electron transfer on a picosecond timescales, return of the electron to the primary donor requires milliseconds [4,5].

2.3 Remarks On The Application Of Hole-Burning

During the past decade, spectral hole-burning has been generally applied to photosynthetic protein-pigment complexes [3-5]. The width of the ZPH, which coincides with the burn frequency, was used to determine the lifetimes of the excited states which

correspond to rapid electronic energy transfer or the primary charge separation. As indicated in Figure 4, a zero-phonon line is accompanied by a phonon side band (PSB). Therefore, the zero-phonon hole (ZPH) is normally assocated with phonon sideband holes (PSBH). The PSBH in the high energy side of the ZPH is referred to as real-PSBH. In contrast to real-PSBH, the pseudo-PSBH lies to lower energy of λ_B (burning wavelength). The pseudo-PSBH are comprised of the bleached zero-phonon lines which absorb the laser light by virtue of the PSB.

Importantly, hole burning reveals the frequencies and coupling strengths (Huang-Rhys factors, i.e., S) of the phonons that couple to the electronic transition [3-5]. Weak electron-phonon coupling (S<1) is the main condition for observing intense zero-phonon lines. As discussed in the previous section, weak phonon coupling corresponds to a small change of the equilibrium configuration of the lattice due to the transition from the ground state to the excited state. Up to now all hole burning studies of the photosynthetic complexes showed weak electron-coupling for antenna [3-5] in contrast to strong coupling for reaction centers. Studies of the neutral excitonic $\pi\pi^*$ dimer states of organic crystals such as anthracene [15] and naphthalene [16], had shown that the exciton-phonon coupling is weak and charge-transfer states of 1:1 donor-acceptor complexes are characterized by very strong electron-phonon coupling [17]. Therefore an excited primary donor (P^*) may possess a significant amount of charge transfer character. Besides the character of strong electron-phonon coupling, the primary donors of bacterial RCs also showed a Franck-Condon progression of low-frequency vibrational mode(s), the so called marker mode(s) [3-5]. The marker mode can be viewed as a pseudolocalized or resonant phonon whose lengthy Franck-Condon progression signals a significant geometry change for the special pair in its excited state. One should notice that the marker mode is not observed in the

system of monomeric chlorophylls. In contrast to bacterial RC, the hole spectra of P680 show a weak contribution from the marker mode (S_{sp}<0.3). This observation reflects the fact that P680 is a monomer-like dimer, as indicated by a longer intra-dimer distance (11Å) of P680 than those of bacterial RCs [18]. The marker mode may originate from the intermolecular vibration of the special pair. Such special properties of the reaction centers

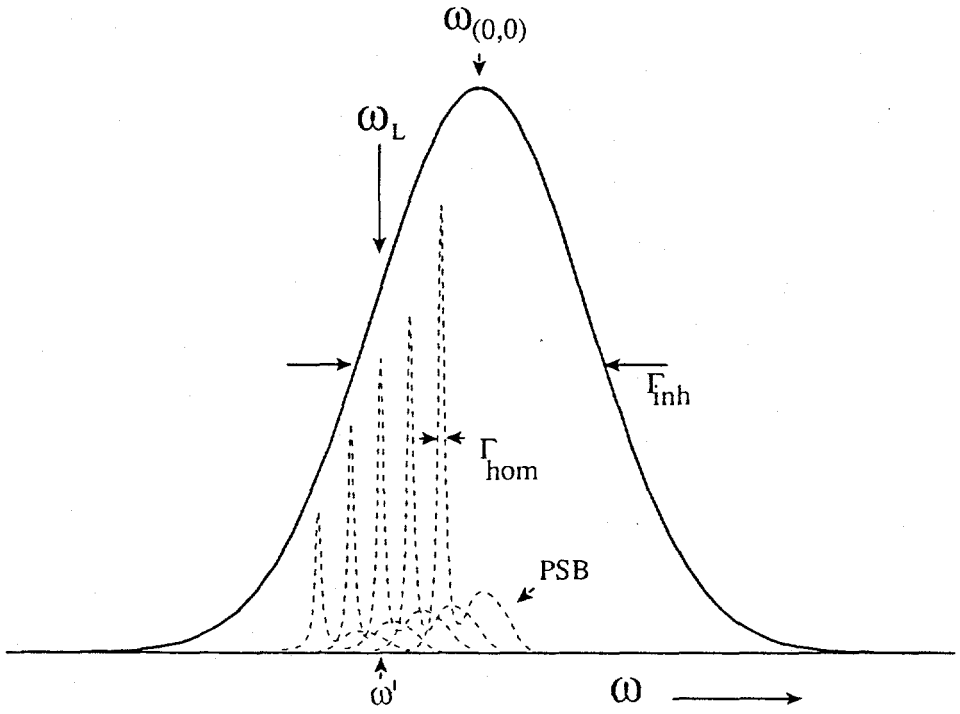

Figure 4. Schematic representation of homogeneous and inhomogeneous broadening. Profiles of the zero-phonon lines (ZPL) and their associated sidebands (PSB) at different frequencies are shown.

have stimulated several works of ultrafast studies [19-21]. The time evolution of the stimulated emission of the primary donor showed a modulation on a picosecond timescale. This phenomenon confirms the existence of the low-frequency nuclear vibrations and implicates the coherent nuclear motion in the primary electron transfer reaction in functional reaction centers.

Spectral hole burning also provides information about inhomogeneous broadening. In the action spectrum the ZPHs were burned under constant burn fluence conditions [22,23]. Assuming that NPHB efficiency is independent of burning frequency, the envelopes of the ZPHs represent the inhomogeneously broadened absorption bands. Nonphotochemical ZPH action spectroscopy has been used to probe weakly-absorbing components of photosynthetic systems (see chapter 4). Due to the inherent "glass-like" structural disorder of proteins, the action spectrum reveals a heterogeneity which is responsible for site inhomogeneous broadening (Γ_{inh}) of the individual absorption bands. Γ_{inh} for chlorophylls and pheophytins of antenna protein-pigment complexes and reaction centers is in the range $\approx$ 50-200 cm^{-1} and is comparable to that observed for chromophores in glasses and polymers [3-5]. Due to the glass-like structure of protein, it is known that the kinetics of electronic energy or electron transfer can be dispersive [24]. To illustrate the relationship between the inhomogeneous broadening and the dispersive kinetics, assume the decay time for a single system to be a single exponential and described as

$$f(t,\omega) = A_\omega e^{-\frac{t}{\tau(\omega)}} \qquad (10)$$

where $\tau(\omega)$ is the lifetime of the system which is isoenergetic with frequency ω. Consider the distribution of heterogeneity to be a Gaussian with a variance σ^2_{inh}. Then

$$g(\omega) = \frac{1}{\sqrt{2\pi}\sigma_{inh}} \exp[-(\omega - \omega_0)^2 / 2\sigma_{inh}^2] \tag{11}$$

where ω_0 corresponds to the position of the maximum. The full-width at half maximum of the Gaussian, i.e., Γ_{inh} is written as

$$\Gamma_{inh} = 2.354\sigma_{inh} \tag{12}$$

The measured kinetic decay is expressed as

$$F(t) = \int f(t,\omega) g(\omega) d\omega \tag{13}$$

Substitution of Eq.10 and Eq.11 into Eq.13 leads to

$$F(t) = \int A_0 e^{-\frac{t}{\tau(\omega)}} \frac{1}{\sqrt{2\pi}\sigma_{inh}} \exp[-(\omega - \omega_0)^2 / 2\sigma_{inh}^2] d\omega \tag{14}$$

As indicated in Eq.14, the measured kinetic decay may be non-single exponential or dispersive due to the inhomogeneous broadening. Whether the system is dispersive or not depends on the magnitudes of inhomogeneous broadening and homogeneous broadening. As discussed by Small et al. [24] (see chapter 3), the average value of rate constant is written as

$$\langle k_{DA} \rangle =$$

$$2\pi V^2 [2\pi(\Gamma^2 + \hat{S}(\sigma^2 + \omega_m^2))]^{-1/2} \exp[-(\Delta E_0 - S\omega_m)^2 / 2[\Gamma^2 + \hat{S}(\sigma^2 + \omega_m^2)] \tag{15}$$

In the case of

$$S(\sigma^2 + \omega_m^2) << \Gamma_{inh}^2, \qquad (16)$$

the system is dispersive.

Whether or not the energy gaps between the Q_y states of different pigments of a particular complex are perfectly correlated (remain the same) between different minimal subunits is particularly interesting. In a highly correlated system the appearance of a sharp ZPH, instead of the whole absorption profile of a acceptor state, represents the presence of a correlation between the donor and acceptor states. Recently, spectral hole burning was used to prove that there is an absence of such correlation for the accessory Chl *a*, active pheophytin *a* and primary electron donor (P680) of the reaction center complex of Photosystem II [25,26].

References

1. Friedrich, J.; Haarer, D. *Angew. Chem. Int. Ed. Engl.* 1984, 23, 113
2. Frauenfelder,H. et al. *J. Phys. Chem.* 1990, 94, 1024
3. Jankowiak, R.; Hayes, J.M.; Small, G.J. *Chem. Rev.* 1993, 93, 1471
4. Jankowiak, R.; Small, G.J. in *The Photosynthetic Reaction Center*, Vol.2, Deisenhofer, J.; Norris, J., Eds.; Academic Press: New York, 1993, p.133
5. Reddy, N.R.S.; Lyle, P.A.; Small, G.J. *Photosyn. Res.* 1992, 31, 167
6. Moerner, W.E., Ed. in *Persistent Spectra Hole-Burning: Science and Applications*; Springer-Verlag: Berlin, 1988
7. Völker,S. in *Relaxation Processes in Molecular Excited States*, Fünfschilling,J., Ed.; Kluwer: Dordrecht, 1989, p.113
8. Jankowiak, R.; Small, G.J. *Science* 1987, 237, 618
9. Gorokhovskii, A.A.; Kaarli, R.K.; Rebane, L.A. *JETP Lett.* 1974, 20, 216

10. Kharlamov, B.M.; Personov, R.I.; Bykovskaya, L.A. *Opt. Commun.* 1974, 12, 191

11. Anderson, P.W.; Halperin, B.J.; Varma, C.M. *Philos. Mag.* 1972, 25, 1

12. Philips, W.A. *J. Low Temp. Phys.* 1972, 7, 351

13. Hayes, J.M.; Small, G.J. *Chem. Phys.* 1978, 27, 151

14. Shu, L.; Small, G.J. *Chem. Phys.* 1990, 141, 447

15. Port, H.; Rund, D.; Small, G.J.; Yakhot, V. *Chem. Phys.* 1979, 39, 175

16. Robinette, S.C.; Small, G.J.; Stevenson, S.H. *J. Chem. Phys.* 1978, 68, 4790

17. Haarer, D. *Chem. Phys. Lett.* 1974, 27, 91

18. Kwa,S.L.S.; Eijckelhoff,C.; van Grondelle,R.; Dekker, J.P. *J. Phys. Chem.* 1994, 98, 7702

19. Vos,M.H.; Rappaport,F.; Lambry,J-C.; Breton,J.; Martin,J-L. *Nature* 1993, 363, 320

20. Vos,M.H.; Jones,M.R.; Hunter,C.N.; Breton,J.; Lambry,J-C.; Martin,J-L. *Biochemistry* 1994, 33, 6750

21. Vos,M.H.; Jones,M.R.; McGlynn,P.; Hunter,C.N.; Breton,J.; Martin,J-L. *Biochim. Biophys. Acta* 1994, 1186, 117

22. Reddy,N.R.S.; Picorel,R.; Small,G.J. J. Phys. Chem. 1992, 96, 6458

23. Reddy, N.R.S.; Cogdell, R.J.; Zhao, L.; Small, G.J. *Photochem. Photobiol.* 1993, 57, 35

24. Small,G.J.; Hayes,J.M.; Silbey,R.J. *J. Phys. Chem.* 1992, 96, 7499

25. Tang,D.; Jankowiak,R.; Seibert,M.; Yocum,C.F.; Small,G.J. *J. Phys. Chem.* 1990, 94, 6519

26. Jankowiak,R.; Tang,D.; Small,G.J.; Seibert,M. *J. Phys. Chem.* 1989, 93, 1649

CHAPTER 3 THEORETICAL BACKGROUND

3.1 Nonadiabatic Electron Transfer Theory

In the application of weak coupling, a nonadiabatic electron transfer theory has been developed by Marcus [1-3], Hopfield [4], Jortner [5] et al., and employed routinely. To illustrate the difference between adiabatic and nonadiabatic cases, the potential energy for nuclear motion for the whole system of donor, acceptor, and surroundings of both cases are plotted against the nuclear configuration (Figure 1). Initial and final equilibrium configurations are labeled as A and B, respectively. In the adiabatic case, the interaction between R and P is so strong that appreciable splitting into curve 1 and 2 is seen at C. In contrast to the adiabatic case, while the nuclear vibrates about the equilibrium position in curve R, passage through C does not usually cause transition from R to P. It is well known that the rate of a transition in the nonadiabatic case from an initial state R to P follows Fermi's golden rule [6]:

$$W_{R\to P} = \frac{2\pi}{\hbar} V^2 (FC), \tag{1}$$

where V is the interaction matrix element between R and P and FC represents the effective Franck-Condon density of states.

To simplify the situation, first consider two harmonic oscillators with the same frequency as shown in Figure 2. Assuming the nuclear vibrations follow Hook's law, the equations of R and P curves are : $V_R = k_H (X - X_A)^2 / 2 + E_R$ and $V_P = k_H (X - X_B)^2 / 2 + E_P$, respectively. As indicated in Figure 2, λ (called the reorganization energy) is the amount of energy required to move the system from initial equilibrium system X_B to X_A.

$$\lambda = V_P(X_A) - V_R(X_A) + \Delta E$$
$$= (k_H/2)(X_A - X_B)^2 \qquad (2)$$

Defining the Huang-Rhys factor (S) as $\lambda/\hbar\omega$, then

$$S = \frac{k_H}{2\hbar\omega}(X_A - X_B)^2 \propto Q^2, \qquad (3)$$

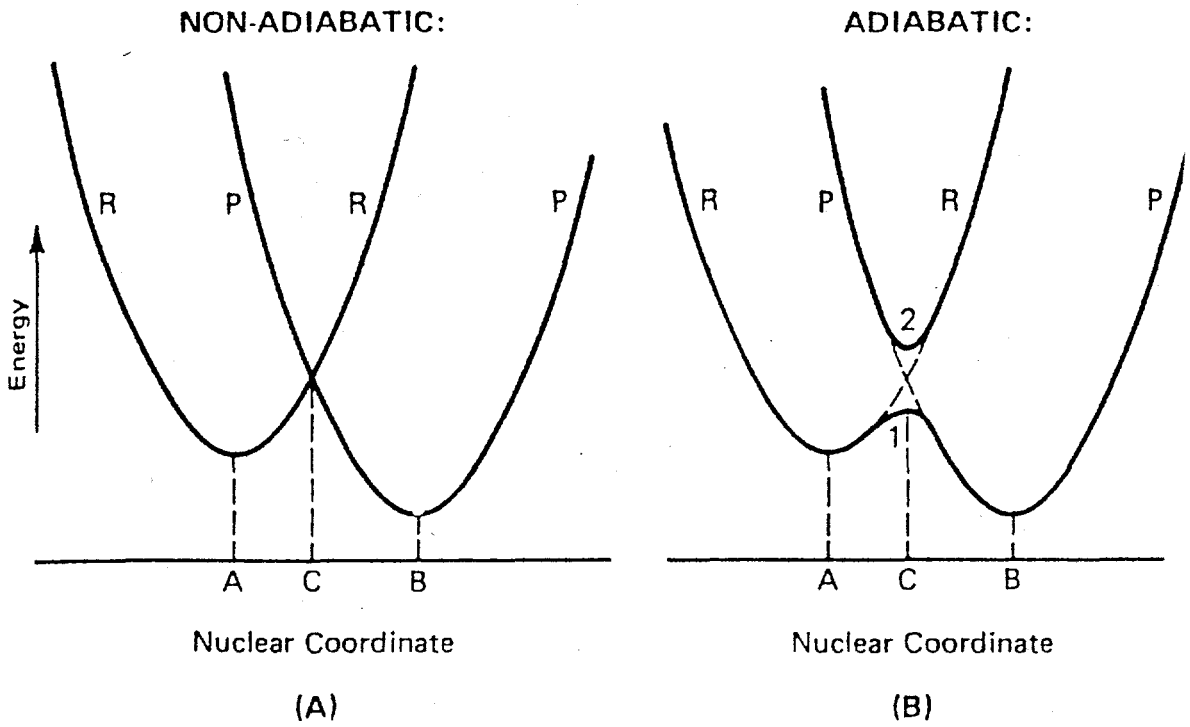

Figure 1. The role of nuclear motion in the cases of non-adiabatic (A) and adiabatic (B) transfer. The initial and final equilibrium configurations are labelled A and B, respectively. In the adiabatic case at the right, interaction between potential curves R and P is so strong that splitting into curves 1 and 2 is seen at C.

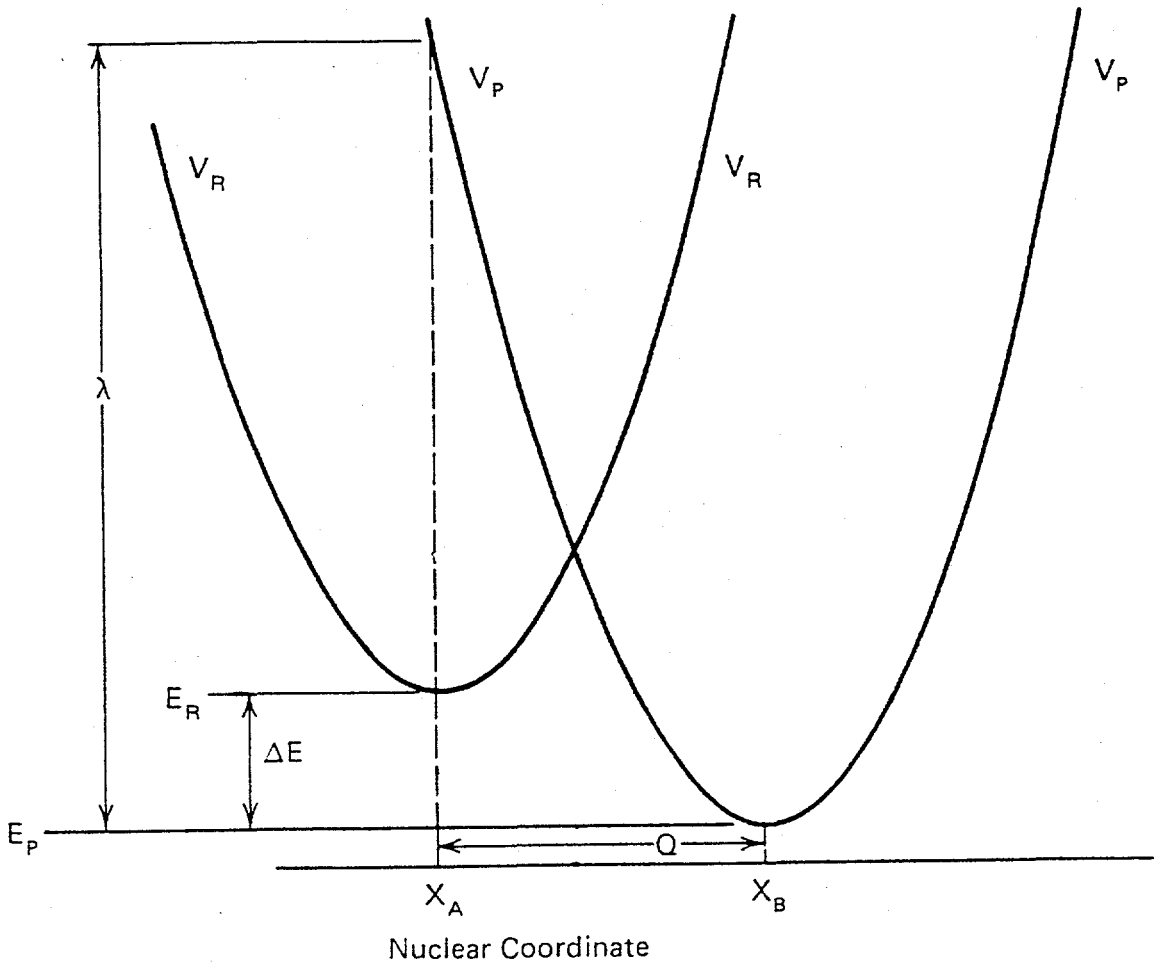

Figure 2. Nuclear motion accompanying non-adiabatic transfer. V_R and V_P represent the nuclear potential curves of the donor and acceptor, respectively. X_A and X_B are the initial and final equilibrium positions, respectively. The reorganization energy, λ, is the amount of energy required to displace the system from X_A to X_B.

where the angular frequency of oscillation, ω, is given by $\omega=\sqrt{\frac{k_H}{M}}$. The Huang-Rhys factor (S) is a measure of the coupling of the nuclear vibrations to the system. If the system consists of a group of oscillators, S is a summation of values for each oscillator. The probability of the transition from R to P is proportional to the square of the 'overlap integral', C(n,n'), between the vibrational state n' in P and the corresponding state n in R. $C^2(n,n')$ is called the Franck-Condon factor given by

$$C^2(n,n') = [\int \chi_n \chi_{n'} dx]^2, \tag{4}$$

where χ_n is the vibrational wavefunction for state n in R, and $\chi_{n'}$ is the wavefunction for state n' in P. x is the oscillator coordinate. At a given temperature, the fraction of systems expected to be in state n of R follows Boltzman distribution under the assumption of thermal equilibrium. Then

$$B(n,T) = e^{-\beta\hbar\omega n}(1-e^{-\beta\hbar\omega})^{-1}, \tag{5}$$

where B(n,T) is the fraction of systems at temperature T. By multiplying each $C^2(n,n')$ by B(n,T) of various n, the FC term in Eq.1 is obtained.

$$FC = \sum_{n=0}^{\infty} C^2(n,n')B(n,T) \tag{6}$$

Substituting Eq.6 into Eq.1 leads to

$$W = A\sum_{n=0}^{\infty} C^2(n,n')B(n,T), \tag{7}$$

where $A = 2\pi V^2 / \hbar^2\omega$. Manneback [7] derived the exact formula for $C^2(n,n')$ with n'=n+p for the case where the frequency does not change.

$$C^2(n,n+p) = n!(n+p)!S^p e^{-S}[\sum_{i=0}^{n} \frac{(-S)^i}{i!(n-i)!(p+i)!}]^2 \qquad (8)$$

To get a more physical feeling for Eq.8, consider the situation as $T \rightarrow 0$ K. At low temperature, almost all molecules occupy the lowest state (n=0). Eq.8 then simplifies to

$$C^2(n=0,p) = \frac{S^p e^{-S}}{p!} \qquad (9)$$

Substitution of Eq.9 and B(n=0, $T \rightarrow 0$ K)=1 into Eq. 6, yields the reduced Franck-Condon factor

$$FC(p) = \frac{S^p e^{-S}}{p!}, \qquad (10)$$

where p=n'-n=n' represents the number of vibrational quanta involved in the transition process. As indicated by Eq.10, the Franck-Condon factor of vibrational quanta (called phonon for the case of lattice vibration) follows the general formula for Poisson statistics [8].

$$P(x,\mu) = \frac{\mu^x e^{-\mu}}{x!} \qquad (11)$$

and

$$\sum_{x=0}^{\infty} P(x,\mu) = e^{-\mu}\sum_{x=0}^{\infty} \frac{\mu^x}{x!} = e^{-\mu}e^{\mu} = 1 \qquad (12)$$

As revealed by Eq.10, the Franck-Condon factor of zero and nonzero-vibrational quanta

processes (p=0) are e^{-S} and $1-e^{-S}$, respectively. Eq.8 is suitable only for the case of two single oscillators with no frequency change. Kubo [9] and Lax [10] further developed the Franck-Condon factor for a system consisting of a group of oscillators which do not change frequency in the form of Eq.13. For a complete derivation, the reader is referred to Devault [11].

$$FC = \frac{1}{2\pi\hbar}\int_{-\infty}^{\infty} dt \exp\{-S[2\bar{n}+1-(\bar{n}+1)e^{i\omega t} - \bar{n}e^{-i\omega t}] - pi\omega t\}, \qquad (13)$$

where S is a summation of values for each oscillator, $\bar{n} = [\exp(\hbar\omega / kT) - 1]^{-1}$ is the average quantum number at thermal equilibrium (in analogy to B(n,T) in Eq.5), and t is a dummy variable. To explain the physical meaning of terms inside exp( ), one starts with the delta function in intergral form

$$\delta(n' - n - p) = \frac{\omega}{2\pi}\int e^{i(n'-n-p)\omega t} dt \qquad (14)$$

which satisfies conservation of energy, i.e.

$$p=n'-n. \qquad (15)$$

As revealed by comparing Eq.13 and 14, the $e^{i\omega t}$ and $e^{-i\omega t}$ terms in Eq.13 correspond to δ (1-p) and δ(-1-p), respectively. That is, $e^{i\omega t}$ and $e^{-i\omega t}$ terms describe the process of the absorption (p=n'-n=1) and emission (p=-1) of one vibrational quantum in a transition. Furthermore, the exp term in Eq.13 describes all the vibrational quanta processes (n'-n=0,1,2...) as indicated by the Taylor expansion series in Eq.16.

$$e^z = 1 + z + \frac{z^2}{2!} + \ldots \qquad (16)$$

Each term of the right hand side of Eq. 16 can be further expanded,

$$z^R = (X+Y)^R = \sum_{T=0}^{R} \frac{X^{R-T}Y^T R!}{(R-T)!T!}. \tag{17}$$

With reference to Eq.13, a more general form of the Franck-Condon factor, modified from Eq.13 for multi-oscillators with different vibrational modes, is usually written as

$$FC = \frac{1}{2\pi\hbar}\int_{-\infty}^{\infty} f(t)e^{-i\Delta Et/\hbar}dt, \tag{18}$$

$$\text{where} \quad f(t) = \exp\{-G + G_+(t) + G_-(t)\} \tag{19}$$

$$G_+(t) = \sum_{\alpha} S_\alpha (\bar{n}_\alpha + 1)e^{i\omega_\alpha t} \tag{20}$$

$$G_-(t) = \sum_{\alpha} S_\alpha \bar{n}_\alpha e^{-i\omega_\alpha t} \tag{21}$$

$$G = G_+(0) + G_-(0). \tag{22}$$

Again, G_+ and G_- represent absorption and emission of one vibrational quantum, respectively. α designates the different modes in a multi-oscillator system and the summations (Σ) are over all modes. Substitution of Eq.18 into Eq.1, yields

$$W = \frac{2\pi}{\hbar}V^2 \frac{1}{2\pi\hbar}\int_{-\infty}^{\infty} f(t)e^{-i\Delta Et/\hbar}dt, \tag{23}$$

where W denotes the trasition rate and V is the interaction matrix element. Eq.23 was the starting point for Small et al. [12] who obtained a simplified but accurate expression for the

rate constant for primary charge separation in the photosynthetic reaction center (RC). The summation terms (Σ) carries the shape of one-vibration quantum (one-phonon) profile were approximated by a Gaussian function, $g(\omega)$, which carries a width of ~2σ

$$g(\omega) = (\sqrt{2\pi}\sigma)^{-1} \exp[-(\omega - \omega_m)^2 / 2\sigma^2] \tag{24}$$

where ω_m represents the mean phonon frequency. The substitution of the summations with a gaussian function, $g(\omega)$, is reasonable, since the hole-burning data [13] indicate that the one-phonon profile is smooth. That is,

$$\sum_{\alpha} S_{\alpha} \approx S \int g(\omega) d\omega \tag{25}$$

Substitution of Eq.25 into Eq.19 leads to

$$f(t) = \exp(-\int g(\omega) S\{(2\bar{n}_{\omega} + 1) - e^{i\omega t}(\bar{n}_{\omega} + 1) - e^{-i\omega t}(\bar{n}_{\omega})\} d\omega) \ . \tag{26}$$

After rearrangement one finds

$$f(t) = \exp[-\int g(\omega) S(2\bar{n}_{\omega} + 1) d\omega + \int g(\omega) S \bar{n}_{\omega} (e^{i\omega t} + e^{-i\omega t}) d\omega + \int g(\omega) S e^{i\omega t} d\omega]. \tag{27}$$

Substitution of the Gaussian function $g(\omega)$, i.e., Eq.24, into Eq.27 followed by integration yields

$$f(t) = \exp(-\hat{S}) \exp[S e^{-\sigma^2 t^2/2} \{(2\bar{n} + 1)\cos\omega_m t + i \sin\omega_m t\}], \tag{28}$$

where $\hat{S}$ is defined as

$$\hat{S} = \int g(\omega) S(2\bar{n}_{\omega} + 1) d\omega \tag{29}$$

$\hat{S}$ is further simplified by employing the mean phonon frequency approximation

$$\hat{S} = S(2\bar{n}+1)$$

$$= S \operatorname{ctnh}(\hbar\omega_m / 2kT) \tag{30}$$

Eq.28 is further approximated by expanding the t-dependent functions in the argument of the exponential, sin and cos and neglecting terms of order higher than t^2.

$$f(t) \approx \exp[-S(2\bar{n}+1)(\sigma^2 + \omega_m^2)t^2/2 + i\omega_m t] \tag{31}$$

Note that Eq.31 originates from Eq.19 which describes all of the phonon processes including the contribution from zero-phonon transition with Franck-Condon factor equal to $\exp(-\hat{S})$. To calculate the contribution of phonon side band mode (n'-n=1,2,...) to energy or electron transfer rate, Eq.31 is multiplied by a factor of $(1-\exp(-\hat{S}))$.

$$f(t) \approx (1 - e^{-\hat{S}}) \exp[-S(2\bar{n}+1)(\sigma^2 + \omega_m^2)t^2/2 + i\omega_m t] \tag{32}$$

Substitution of Eq.32 into Eq.23 and taking the Fourier transform using

$$\frac{1}{\sqrt{2\pi}} \int e^{-Pt^2} e^{i\alpha t} dt = \frac{1}{\sqrt{2P}} e^{-\alpha^2/4P} \tag{33}$$

leads to

$$W = 2\pi V^2(1-e^{-\hat{S}})[(2\pi\hat{S}(\sigma^2+\omega_m^2))^{-1/2}e^{-\frac{(\Delta E-S\omega_m)^2}{2\hat{S}(\sigma^2+\omega_m^2)}}] \quad (34)$$

Note that Eq.19 is the form suitable for harmonic oscillators with no frequency change between initial (donor) and final (acceptor) states. That is, Eq.34 assumes the phonons created by the energy or electron transfer process have no frequency change, and are shared entirely between donor and acceptor state. For delocalized phonon the assumption of no frequency change is an excellent one. Eq.34 was used to calculate the electron transfer rate constant for a single reaction center (RC).

$$k_{DA} = 2\pi V^2(1-e^{-\hat{S}})[(2\pi\hat{S}(\sigma^2+\omega_m^2))^{-1/2}e^{-\frac{(\Delta E-S\omega_m)^2}{2\hat{S}(\sigma^2+\omega_m^2)}}] \quad (35)$$

In the strong electron-phonon coupling limit ($\hat{S}>1$), the rate constant for single RC can be approximated as

$$k_{DA} = 2\pi V^2[(2\pi\hat{S}(\sigma^2+\omega_m^2))^{-1/2}e^{-\frac{(\Delta E-S\omega_m)^2}{2\hat{S}(\sigma^2+\omega_m^2)}}], \quad (36)$$

where ΔE is the electronic energy gap and V is the electronic coupling matrix element between the donor and acceptor states. For a Gaussian distribution of ΔE values centered at ΔE_0, the average value for the rate is [14]

$$< k_{DA} >=$$

$$2\pi V^2[2\pi(\Gamma^2+\hat{S}(\sigma^2+\omega_m^2))]^{-1/2}\exp[-(\Delta E_0 - S\omega_m)^2/2[\Gamma^2+\hat{S}(\sigma^2+\omega_m^2)], \quad (37)$$

where 2Γ is the width of the normal distribution for ΔE. As pointed out by Small et al. [12,14] Γ^2 and $\hat{S}(\sigma^2+\omega_m^2)$ can be viewed as terms associated with inhomogeneous and

homogeneous broadening, respectively. In the case of

$$S(\sigma^2+\omega_m^2) >> \Gamma^2 \tag{38}$$

the average rate constant $\langle k_{DA} \rangle$ is simplified to

$$< k_{DA} >= 2\pi V^2[(2\pi \hat{S}(\sigma^2+\omega_m^2))^{-1/2} e^{-\frac{(\Delta E_0 - S\omega_m)^2}{2\hat{S}(\sigma^2+\omega_m^2)}}] \tag{39}$$

That is, the kinetics are non-dispersive as indicated by $\langle k_{DA} \rangle = k_{DA}(\Delta E = \Delta E_0)$. Further application of Eq.37 in the high pressure studies of a Photosystem II reaction center will be discussed later in Chapter seven.

3.2 Theory Of Molecular Excitons

To illustrate the theory of molecular excitons, consider the case of a one-dimensional array of N identical molecules which are located at a distance r from each other. The energy states of an isolated molecule are determined by

$$(H - E^i)\varphi^i = 0 \ , \tag{40}$$

where i corresponds to the ground state (i=0) or excited state (i=e) of the molecule. For simplicity, non-degenerate levels of the molecule are assumed. In the case of N molecules, Eq.40 is rewritten as

$$(\sum_{n=1}^{N} H_n + \frac{1}{2}\sum_{n,m}{}' V_{nm} - E)\phi^i = 0 \ , \tag{41}$$

where V_{nm} is the matrix element of interaction between molecules n and m. $\sum_{n,m}{}'$ is the summation of all terms except n=m. The wavefunction of the ground state of the system of

N molecules can be written in the form of

$$\psi^0 = \prod_{n=1}^{N} \varphi_n^0 \,. \tag{42}$$

From first-order perturbation theory [15], the energy of the ground state of the system of N identical molecules is equal to

$$E^0 = NE_u^0 + \frac{1}{2}\int \psi^{0*} \sum_{n,m}{}' V_{nm}\psi^0 d\tau \,, \tag{43}$$

where E_u^0 is the energy of the ground state of an unpertubed molecule. An excited state can be written in a similar manner if it is assumed that only one molecule is in an excited state. Then, for molecule at site n excited, one has

$$\phi_n^e = \varphi_n^e \prod_{m(m\neq n)} \varphi_m \,, \tag{44}$$

where e denotes the excited state and ϕ_n^e is the excited state wavefunction with the excitation energy localized at nth molecule. It is clear from the pertubation theory that the wavefunctions of the excited states result in an N-fold degeneracy if the interactions among the states in which the excitation is at different sites are negligible. The first order energy correction of ϕ_n^e is

$$D = \frac{1}{2}\int \phi_n^{e*} \sum_{n,m}{}' V_{nm}\phi_n^e d\tau \,. \tag{45}$$

Eq.45 does not account for the interactions among the states. Furthermore, the states (Eq.44) are not stationary states of the system if there are nonvanishing matrix elements among these states. As shown in Eq.46, the interaction energy among states is

$$M = \frac{1}{2}\int \phi_n^{e*} \sum_{n,m}{}' V_{nm} \phi_m^e d\tau \ . \tag{46}$$

To properly describe the coupling among states, the wavefunctions of the excited states are rewritten in the form of a linear combination of the states. Then

$$\psi^e = \frac{1}{\sqrt{N}} \sum_n b_n \phi_n^e \ , \tag{47}$$

where ψ^e represents the wavefunction of the delocalized excited state. In order to have a better understanding of the exciton theory, consider a model of two identical molecules coupled by an interaction V. The Hamiltonian of this system is simplified as

$$H = H_1 + H_2 + V, \tag{48}$$

where H_1 and H_2 are the Hamiltonians of the isolated molecules and V is the interaction operator between two molecules. As indicated by Eq.47, the wavefunction of the delocalized excited state is a linear combination of the localized wavefunctions with excitation energy localized at first and second molecules, respectively. Then

$$\psi_i^e = a_{1i} \varphi_1^e \varphi_2 + a_{2i} \varphi_1 \varphi_2^e \ , \tag{49}$$

where ψ_i^e represents the wavefunctions of the stationary excited states. i=1 or 2 denotes the first or second stationary excited states of the system of two molecules. The wavefunctions of stationary states must be orthogonal to each other and normalized, i.e., they must satisfy the condition:

$$\int \psi_i^{e*} \psi_j^e d\tau = \delta_{ij} \ . \tag{50}$$

Substitution of Eq.49 into Eq.50 leads to the solutions:

$$\psi_1^e = \psi^+ = \frac{1}{\sqrt{2}}(\varphi_1^e\varphi_2 + \varphi_1\varphi_2^e) \tag{51}$$

and

$$\psi_2^e = \psi^- = \frac{1}{\sqrt{2}}(\varphi_1^e\varphi_2 - \varphi_1\varphi_2^e) \ , \tag{52}$$

where ψ^+ and ψ^- are the wavefunctions of the excited dimer states. The first order energy correction of the excited states are

$$\langle\psi^\pm|V|\psi^\pm\rangle =$$

$$\frac{1}{2}\{[\int\varphi_1^e\varphi_2 V\varphi_1^e\varphi_2 d\tau + \int\varphi_1\varphi_2^e V\varphi_1\varphi_2^e d\tau] \pm [\int\varphi_1^e\varphi_2 V\varphi_1\varphi_2^e d\tau + \int\varphi_1\varphi_2^e V\varphi_1^e\varphi_2 d\tau]\} \ . \tag{53}$$

The physical meaning of Eq.53 is explained as follows. The first two terms of the right hand side of Eq.53 represent the interaction energy between the excited molecule and its neighboring molecule. The third and fourth terms mean the excitation transfer between two molecules induced by the coupling term V and cause the dimer splitting or exciton splitting in the excited states. The energy difference between ψ^+ and ψ^- is

$$\Delta E = 2[\int\varphi_1^e\varphi_2 V\varphi_1\varphi_2^e d\tau + \int\varphi_1\varphi_2^e V\varphi_1^e\varphi_2 d\tau] \ . \tag{54}$$

With reference to Eq.45-47, the physical meaning of Eq.47 can be explained as the excitation energy which is no longer localized at nth molecules (delocalized exciton). As discussed above, Eq.46 determines the exchange of excitation between the nth and mth

molecules. That is, M of Eq.46 reflects the excitation transfer time τ_t [16]. D of Eq.45 represents the interaction of the excited nth molecule with all the other normal molecules [16]. The Hamiltonian for delocalized exciton is conveniently written as [16,17]

$$H_{EX} = \sum_n [(E_u + \sum_m{}' D_{nm}) B_n^+ B_n + \sum_m{}' M_{nm} B_m^+ B_n] , \tag{55}$$

where the operators B_n^+ and B_n are the creation and annihilation operators for the nth site and E_u is the excitation energy of an isolated molecule. Again D represents the interaction between the excited nth molecule and all other ground state molecules and M represents the excitation transfer from the nth molecule to the mth molecule. H_{EX} is a function of the lattice configuration by virtue of the fact that the matrix element D_{nm} and M_{nm} are. D_{nm} and M_{nm} may be decomposed into a power series of the displacement R relative to the equilibrium positions of the molecules.

$$D_{nm}(R) = D_{nm}(0) + D_{nm}(1) + \ldots \tag{56}$$

$$M_{nm}(R) = M_{nm}(0) + M_{nm}(1) + \ldots \tag{57}$$

where

$$D_{nm}(1) = \sum_\alpha [R_{n\alpha} (\frac{\partial D_{nm}}{\partial R_{n\alpha}})_0 + R_{m\alpha} (\frac{\partial D_{nm}}{\partial R_{m\alpha}})_0] \tag{58}$$

$$M_{nm}(1) = \sum_\alpha [R_{n\alpha} (\frac{\partial M_{nm}}{\partial R_{n\alpha}})_0 + R_{m\alpha} (\frac{\partial M_{nm}}{\partial R_{m\alpha}})_0] \tag{59}$$

and α respresents the six degrees of freedom of the molecules (three for translation and

three for rotation). Obtained from Eq.57 and Eq.58, the Hamiltonian of exciton-phonon coupling is written as

$$H_{EX-PH}^{(1)} = \sum_n \sum_m{}' B_m^+ B_n \sum_\alpha [(R_{n\alpha}(\frac{\partial M_{nm}}{\partial R_{n\alpha}})_0 + R_{m\alpha}(\frac{\partial M_{nm}}{\partial R_{m\alpha}})_0] \tag{60}$$

$$H_{EX-PH}^{(2)} = \sum_n \sum_m{}' B_n^+ B_n \sum_\alpha [(R_{n\alpha}(\frac{\partial D_{nm}}{\partial R_{n\alpha}})_0 + R_{m\alpha}(\frac{\partial D_{nm}}{\partial R_{m\alpha}})_0] \tag{61}$$

To have a clearer understanding, consider the case of two identical molecules, i.e., D (donor) and A (acceptor). As indicated in Eq.55, the Hamiltonian of the dimer for the delocalized exciton is written as

$$H_{EX} = 2E_u + D_{DA}(B_D^+ B_D) + D_{AD}(B_A^+ B_A) + M_{DA} B_A^+ B_D + M_{AD} B_D^+ B_A \ . \tag{62}$$

D and A are identical molecules, so

$$D_{DA} = D_{AD} = D \tag{63}$$

and $$M_{DA} = M_{AD} = M \quad . \tag{64}$$

Substitution of Eq.63 and Eq.64 into Eq.62, we have

$$H_{EX} = 2E_u + D(B_D^+ B_D + B_A^+ B_A) + M(B_A^+ B_D + B_D^+ B_A). \tag{65}$$

To illustrate the physical meaning of M, consider the operation of the creation and annihilation operators.

$$MB_A^+B_D\left|D^eA\right\rangle = MB_A^+\left|DA\right\rangle = M\left|DA^e\right\rangle \tag{66}$$

and

$$MB_D^+B_A\left|DA^e\right\rangle = MB_D^+\left|DA\right\rangle = M\left|D^eA\right\rangle. \tag{67}$$

As revealed by Eq.66 and Eq.67, M represents the resonance-energy transfer matrix elements between two molecules, i.e., from D^eA to DA^e.

The matrix element D determines the extent of the lattice distortion which may occur at and around a given excitation site (donor or acceptor). The excited and normal molecules act with different forces upon their neighbors. A change in the force of interaction between neighboring molecules upon the excitation of one molecule in the system sometimes may cause a displacement of molecules to new equilibrium positions. The displacement of the molecules may involve the distortion of the lattice. The displacement time (τ_d) of molecules from the old equilibrium positions depends on the change in the force of the interaction of a molecule with neighboring ones upon excitation of the molecule. With reference to Eq.58, the distortion arises from the first order term of D, that is, from

$$D(1) = \sum_{\alpha}[R_{D\alpha}(\frac{\partial D_{DA}}{\partial R_{DA}})_0 + R_{A\alpha}(\frac{\partial D_{DA}}{\partial R_{A\alpha}})_0] \ . \tag{68}$$

The subscript 0 designates evaluation at the ground-state configuration. For simplicity, consider the case of a dimer system with strong dispersion coupling (D) which must be dealt with first before energy transfer (M) is considered. Note that the displacement of the molecules can be expressed as the ground-state phonon coordinate [17,18]. Then

$$D(1) = \sum_{q} Q_q(\frac{\partial D_{DA}}{\partial Q_q})_0 \ , \tag{69}$$

where Q_q is the phonon coordinate associated with mode q. To reach the thermal equilibrium among exciton levels, downward energy cascading between exciton levels (ψ^+ and ψ^-) is accompanied by emission of phonons (Davydov mechanism). To have a clear physical understanding, assume Q_p to be the promoting mode. It is convenient to express the phonon coordinate in terms of creation and annihilation operators [17]. Then

$$Q_p = (\frac{\hbar}{2\omega_p})^{1/2}(b + b^+) \tag{70}$$

The interaction matrix element of downward energy cascading accompanied by the absorption of one phonon of the lattice takes the following form in the first order of perturbation:

$$\begin{aligned}
&\left\langle \psi^- m_{n_p+1} \middle| Q_p (\frac{\partial D_{DA}}{\partial Q_p})_0 \middle| \psi^+ m_{n_p} \right\rangle \\
&= \left\langle m_{n_p+1} \middle| (\frac{\hbar}{2\omega_p})^{1/2}(b + b^+) \middle| m_{n_p} \right\rangle \left\langle \psi^- \middle| (\frac{\partial D_{DA}}{\partial Q_p})_0 \middle| \psi^+ \right\rangle \\
&= (\frac{\hbar}{2\omega_p})^{1/2}(n_p + 1)^{1/2} \left\langle \psi^- \middle| (\frac{\partial D_{DA}}{\partial Q_p})_0 \middle| \psi^+ \right\rangle
\end{aligned} \tag{71}$$

where m_{n_p} and m_{n_p+1} represent the phonon states before and after absorbing one phonon, respectively. The first term represents the absorption of one phonon of the promoting mode, and the second term represents the downward energy cascading from ψ^+ to ψ^- state. In the case of a promoting mode of frequency ω_p contributing to the process of the energy cascading, the enregy gap left for the delocalized phonons to fulfill is equal to

$$\Delta E' = \Delta E - \hbar\omega_p \, . \tag{72}$$

With reference to Eq.35 of section 3.1, the rate constant with the summation of all phonon modes is rewritten as

$$k = 2\pi(\frac{\partial D_{DA}}{\partial Q_p})_0^2(\frac{\hbar}{2\omega_p})(n_p+1)(1-e^{-\hat{S}})[(2\pi\hat{S}(\sigma^2+\omega_m^2))^{-1/2}e^{-\frac{(\Delta E-\hbar\omega_p-S\omega_m)^2}{2\hat{S}(\sigma^2+\omega_m^2)}}], \quad (73)$$

where $(\frac{\hbar}{2\omega_p})(n_p+1)$ is the transition probability of the promoting mode, as indicated in Eq.71. Further applications of Davydov mechanism in photosynthesis will be discussed in Chapter four.

3.3 Theory Of Hole Profile

Consider the absorption of light from the initial electronic state i leading to the final electronic state j. The absorption cross-section is written [19] as

$$\sigma(\Omega) = \frac{4\pi^2\Omega}{\hbar c}\sum_n\sum_{n'}|\langle j,n'|\mu|i,n\rangle|^2\delta(\Omega-(E_{j,n'}-E_{i,n})/\hbar), \quad (74)$$

where μ is the dipole moment. n' and n denote the vibrational levels of the final and initial states, respectively. With the allowance for the homogeneous broadening, replace the delta function with a Lorentzian function $l_{n'n}$. Eq.74 is rewritten as

$$\sigma(\Omega) = \sum_\alpha\frac{4\pi^2\Omega}{\hbar c}\sum_n\sum_{n'}|\langle j,n'|\mu|i,n\rangle|^2 l_{n'n}(\Omega-(E_{j,n'}-E_{i,n})/\hbar), \quad (75)$$

where α denotes the pnonon modes. With the Condon approximation, the matrix element in Eq.75 becomes

$$|\langle j,n'|\mu|i,n\rangle|^2 = |\langle j|\mu|i\rangle|^2|\langle n'|n\rangle|^2 \quad (76)$$

Recall that $|\langle n'|n\rangle|^2$ is the Franck-Condon factor, $C^2(n,n')$, discussed in section 3.1. With the benefit of the Condon approximation, the theory of nondiabatic transfer can be utilized for the development of the theory of hole profiles. Substitution of Eq.76 into Eq.75 leads to

$$\sigma(\Omega) \propto \sum_{\alpha} \sum_{n} \sum_{n'} |\langle n'|n\rangle|^2 l_{n'n}(\Omega - (E_{j,n'} - E_{i,n})/\hbar) \tag{77}$$

To have a better physical feeling, consider a low temperature case (T→0K), in which only the n=0 term is left. Eq.77 is rewritten as

$$\sigma(\Omega) \propto \sum_{\alpha} \sum_{n'} C^2(n=0,n') l_{n'0}(\Omega - (E_{j,n'} - E_{i,0})/\hbar) \tag{78}$$

With reference to section 1.1, the Franck-Condon factor of the transition from n=0 to n' is given by a Poisson distribution.

$$C^2(n=0,n') = C^2(p) = \frac{S^p e^{-S}}{p!}\ , \tag{79}$$

where p=n'-n is equal to n' at the low temperature limit. Substitution of Eq.79 into Eq.78 leads to

$$\sigma(\Omega) \propto \sum_{\alpha} \sum_{p=0}^{\infty} \frac{e^{-S}S^p}{p!} l_{n'0}(\Omega - (E_{j,n'} - E_{i,0})/\hbar) \tag{80}$$

The zero-phonon line (ZPL) frequency is a Lorentzian centered at υ. υ is defined as

$$\upsilon = (E_{j,0} - E_{i,0})/\hbar. \tag{81}$$

Substitution of Eq.81 into Eq.80 leads to

$$\sigma(\Omega) \propto \sum_{\alpha} \sum_{p=0}^{\infty} \frac{e^{-S} S^p}{p!} l_{n'0}(\Omega - \upsilon - n' \omega_\alpha) \tag{82}$$

Because the frequencies of the phonons are close together, the sum ($\sum_{\alpha}$) of the Lorentzian functions becomes a smooth function of frequency with a one-phonon spectrum centered at $\upsilon + \omega_m$ and the n'-phonon centered at $\upsilon + n' \omega_m$. Eq.82 is rewritten as

$$\sigma(\Omega) \propto \sum_{p=0}^{\infty} \frac{e^{-S} S^p}{p!} l_p(\Omega - \upsilon - p\omega_m), \tag{83}$$

where ω_m is the mean phonon frequency. The p values of 0, 1, 2,... correspond to zero-, one-, two-, ... phonon transitions. The p-phonon lineshape (l_p) is the result of convoluting one-phonon profile (l_1) p-times with itself. Note that the inhomogeneous distribution of various sites is not considered in Eq.83. Define the single site absorption profile in the low temperature limit [13] as

$$L(\Omega - \upsilon) = \sum_{p=0}^{\infty} \frac{e^{-S} S^p}{p!} l_p(\Omega - \upsilon - p\omega_m). \tag{84}$$

The absorption spectrum is the integral (or summation) of the single-site absorption profiles with a Gaussian distribution of ZPL frequencies. Then

$$A_0(\Omega) = \int d\upsilon N_0(\upsilon - \upsilon_m) L(\Omega - \upsilon) , \tag{85}$$

where $N_0(\upsilon - \upsilon_m)$ is the distribution of ZPL frequencies centered at frequency υ_m and $A_0(\Omega)$ is the absorption spectrum before burning. Substitution of Eq.84 into Eq.85 leads

to

$$A_0(\Omega) = \sum_{p=0}^{\infty} \frac{e^{-S} S^p}{p!} \int d\upsilon N_0(\upsilon - \upsilon_m) l_p(\Omega - \upsilon - p\omega_m). \quad (86)$$

Let the laser intensity and the quantum yield of hole burning equal to I and ϕ, respectively. Then following a burn for time τ [22]

$$N_\tau(\upsilon - \upsilon_m) = N_0(\upsilon - \upsilon_m) \exp[-\sigma I \phi \tau L(\omega_B - \upsilon)] , \quad (87)$$

where ω_B and σ are the laser burn frequency and the optical cross section, respectively. The absorption spectrum following hole burning at a frequency ω_B for a time τ is written as

$$A_\tau(\Omega) = \int d\upsilon N_\tau(\upsilon - \upsilon_m) L(\Omega - \upsilon) . \quad (88)$$

Substitution Eq.87 into Eq.88 leads to

$$A_\tau(\Omega) = \sum_{p=0}^{\infty} \frac{e^{-S} S^p}{p!} \int d\upsilon N_0(\upsilon - \upsilon_m) \exp[-\sigma I \phi \tau L(\omega_B - \upsilon)]$$

$$\times l_p(\Omega - \upsilon - p\omega_m). \quad (89)$$

The hole spectrum $H(\Omega)$ is obtained as the difference between the absorption spectra of after-burn (Eq.89) and pre-burn (Eq.86).

$$H(\Omega) = A_\tau(\Omega) - A_0(\Omega) \quad (90)$$

Eq.84 is the expression of the single site absorption profile valid in the low temperature

limit. To extend the theory of hole profile to arbitrary temperatures [20], begin with the general form of Franck-Condon factor [11,21] mentioned in previous section (section 3.1).

$$FC = \frac{1}{2\pi\hbar}\int_{-\infty}^{\infty} f(t)e^{-i\Delta Et/\hbar}dt \tag{91}$$

where $f(t) = \exp\{-G + G_+(t) + G_-(t)\}$ (92)

$$G_+(t) = \sum_\alpha S_\alpha(\bar{n}_\alpha + 1)e^{i\omega_\alpha t} \tag{93}$$

$$G_-(t) = \sum_\alpha S_\alpha \bar{n}_\alpha e^{-i\omega_\alpha t} \tag{94}$$

$$G = G_+(0) + G_-(0) \tag{95}$$

G_+ and G_- represent absorption and emission of one phonon [11], respectively. The parameter t is simply a dummy variable. As indicated in Eq.93 and 94, $S_+ = (\bar{n}+1)S$ and $S_- = \bar{n}S$ correspond to absorption and emission of one phonon, respectively. At low temperature limit ($\bar{n} \to 0$), only S_+ (or G_+) nonvanishes. The term of exp in Eq.92 can be viewed as multi-phonon processes as revealed in the expansion of a Taylor series.

$$\exp[G_+ + G_-] = \sum_{p=0}^{\infty}\frac{[G_+ + G_-]^p}{p!}$$

$$= \sum_{p=0}^{\infty}\sum_{p'=0}^{p}\frac{[G_+]^{p-p'}[G_-]^{p'}}{(p-p')!p'!} \tag{96}$$

Substituting Eq.96 into Eq.92 and Eq.91 and performing the integration gives

$$FC = e^{-\sum_{\alpha} S_{\alpha}(2\bar{n}_{\alpha}+1)} \sum_{p=0}^{\infty} \sum_{p'=0}^{p} \sum_{\alpha} \frac{[S_{\alpha}(\bar{n}_{\alpha}+1)]^{p-p'}[S_{\alpha}\bar{n}_{\alpha}]^{p'}}{(p-p')!p'!}$$

$$\times \delta[-\frac{\Delta E}{\hbar} + \sum_{\alpha} \omega_{\alpha}[p-2p']] \qquad (97)$$

In the case of low temperature ($G_- \rightarrow 0$), Eq.96 is rewritten as

$$\exp[G_+ + G_-]$$

$$= \exp[G_+] = \sum_{p=0}^{\infty} \frac{G_+^p}{p!} \qquad (98)$$

Substituting $\bar{n} \rightarrow 0$ and Eq.98 into Eq.92 and Eq.91, we have

$$FC = e^{-\sum_{\alpha} S_{\alpha}} \sum_{p=0}^{\infty} \sum_{\alpha} \frac{S_{\alpha}^p}{p!} \delta[-\frac{\Delta E}{\hbar} + p\omega_{\alpha}]$$

$$= e^{-S} \sum_{p=0}^{\infty} \frac{S^p}{p!} \delta[-\frac{\Delta E}{\hbar} + p\omega_m]. \qquad (99)$$

Eq.99 shows that Eq.97 is reduced to the Poisson distribution at low temperature limit. That is, Eq.97 is the general form of Franck-Condon factor for arbitrary temperatures. In analogy to Eq.84, the delta function is replaced by a line shape function. The single site absorption profile for arbitrary temperature is written as

$$L(\Omega - \upsilon) = e^{-\sum_{\alpha} S_{\alpha}(2\bar{n}_{\alpha}+1)} \sum_{p=0}^{\infty} \sum_{p'=0}^{p} \sum_{\alpha} \frac{[S_{\alpha}(\bar{n}_{\alpha}+1)]^{p-p'}[S_{\alpha}\bar{n}_{\alpha}]^{p'}}{(p-p')!p'!}$$

$$\times l_{pp'}(\Omega - \upsilon - (p-2p')\omega_{\alpha}) \qquad (100)$$

Consequently, following the same procedure as the case of low temperature (Eq.85-90), the equation of hole profile for arbitrary temperature is obtained. Applications of the theory of hole profile to photosynthesis will be discussed in later chapters (see chapter 5 to chapter 7)

References

1. Marcus,R.A. *J Chem. Phys.* 1956, 24, 966
2. Marcus,R.A. *J. Chem. Phys.* 1965, 43, 679
3. Marcus,R.A.; Sutin,N. *Biochim. Biophys. Acta* 1985, 811, 265
4. Hopfield,J.J. *Proc. Natl. Acad. Sci. USA* 1974, 71, 3640
5. Jortner,J. *J. Chem. Phys.* 1976, 64, 4860
6. Atkins,P.W. in *Molecular Quantum Mechanics*; Oxford: London, 1983, p.198
7. Manneback,C. *Physica Grav.* 1951, 17, 1001
8. Bevington,P.R.; Robinson,D.K. in *Data Reduction and Error Analysis for the Physical Sciences*; McGraw-Hill: New York, 1992, p.24
9. Kubo,R. *Phys. Rev.* 1952, 86, 929
10. Lax,M. *J. Chem. Phys.* 1952, 20, 1752
11. DeVault,D. *Quart. Rev. of Biophys.* 1980, 13., 387
12. Small,G.J.; Hayes,J.M.; Silbey,R.J. *J. Phys. Chem.* 1992, 96, 7499
13. Hayes,J.M.; Gillie,J.K.; Tang,D.; Small,G.J. *Biochim. Biophys. Acta* 1988, 932, 287
14. Kolaczkowski,S.V.; Hayes,J.M.; Small, G.J. *J. Phys. Chem.* 1994, 98, 13418
15. Davydov,A.S. in *Quantum Mechanics*; NEO Press: Ann Arbor, 1966, p.538

16. Davydov,A.S. in *Theory of Molecular Excitons*; Plenum: New York, 1971

17. Johnson,C.K.; Small,G.J. in *Excited States*, Vol.6; Lim,E.C.,Ed.; Academic Press: New York, 1982, p.97

18. Clark,M.; Craig,D.P.; Dissado,L.A. *Mol. Cryst. Liq. Cryst.* 1978, 44, 309

19. Pryce,M.H.L. in *Phonons in Perfect Lattices and Lattices with Point Defects*; Stenenson,R.W.H., Ed.; Oliver and Boyd: London, 1965, p.403

20. Hayes,J.M.; Lyle,P.A.; Small,G.J. *J. Phys. Chem.* 1994, 98, 7337

21. Englman,R. in *Non-Radiative Decay of Ions and Molecules in Solids*; North-Holland: Amsterdam, 1979

22. Friedrich,J.; Haarer,H. in Optical Spectroscopy of Glasses; Zschokke,I., Ed.; D. Reidel: Dordrecht, 1986, p.149

CHAPTER 8 GENERAL CONCLUSIONS

Considerable progress has been made towards an understanding of the excited electronic state structure and primary charge separation dynamics of the PS II RC. The present work establishes the importance of CP47 contamination and the 684 nm absorbing Chl *a* in preparations containing, on average, 5 and 6 Chl *a* molecules per RC complex. Our previous and present measurements of the $^1P680^*$ lifetime, together with the time domain data, indicate that the 684 nm Chl *a* do not play a role in primary charge separation. However, both the 684 nm Chl *a* and CP47 contamination should be expected to complicate the interpretation of energy transfer data. Therefore, in future studies of energy transfer dynamics and electron-phonon coupling, attention should be focused on 4 Chl *a*-RC preparations which contain negligibly low amounts of CP47, 684 nm Chl *a* and non-native Chl *a* absorbing near 670 nm.

The 684 nm absorbing Chl *a* contribute to the additional Chl *a* are of the linker type, serving to shuttle energy from the proximal antenna complex to the reaction center. Implicit in this model is that the 684 nm Chl *a* communicate with the primary electron donor Chl *a* (P680) via energy transfer and that the resulting detrapping of the Q_y-state of the 684 nm Chl *a* should depend strongly on temperature. Temperature dependent transient hole spectra are presented that are in complete accord with this prediction. Theoretical calculations on the kinetics and temperature dependence of the hole profile of the 680 nm absorption band are presented and provide convincing support for the linker model. The data are argued to be inconsistent with other models.

In the CP47 protein complex, attention is focused on the lower energy chlorophyll *a* Q_y-states. On the basis of the analysis of the hole and static fluorescence spectra at

4.2K, the lowest energy state of CP47 was found to be at 690 nm. The 690 nm and 687 nm states are excitonically correlated and correspond to an excitonically coupled dimer.

It has demonstrated, for the first time, that pressure can have a pronounced effect on primary charge separation of a reaction center. The 4.2K lifetime of $P680^*$, the primary donor state, increases from 2.0 ps to 7.0 ps as pressure increases from 0.1 to 267 MPa. While this effect is plastic, the pressure induced effects on the Q_y-absorption and non-line narrowed P680 hole profile are elastic. The latter observation, together with the observation that the linear electron-phonon coupling of the $P680^* \leftarrow P680$ transition is, at most, weakly dependent on pressure, allowed us to eliminate $P680^*$ and the electronic coupling V as sources for the plastic pressure dependence of the primary charge separation kinetics. Within the standard model of primary charge separation, it was then possible to focus on the acceptor state ($P680^+Pheo^-$ and $P680^+Chl^-$ for the superexchange and two-step mechanisms, respectively). It was found that the pressure dependence could be explained with a linear pressure shift of ≈ 1 cm^{-1}/MPa in magnitude for the acceptor state. (The data and calculations do not permit a distinction between the superexchange and two-step mechanisms.) We emphasize that the PS II RC appears to be an ideal candidate for more detailed studies of the pressure dependence of primary charge separation.

ACKNOWLEGEMENTS

It is a pleasure rather than a duty to record my thanks to my advisors, many friends, and organizations for their guidance, help, encourgement, and financial assistance during my years of research. In particular I want to mention Professor Small whose steady advice and rigorous criticism prevented me from making many mistakes. The work contained here is certainly more a product of his efforts than of mine. I am grateful to Professor Struve who allows me to choose him as one of the coadvisors. A large thank you goes to Dr. Ryszard Jankowiak and Dr. N.Raja.S. Reddy for discussions and experimental guidance in my research projects of Photosystem II. Thanks must go to Dr. John M. Hayes for the use of the hole simulation programs.

Life in Ames was enriched not only by the facilities of the University, but also by many friendships. First in Prof. Small's group I would like to thank Dr. Freek Ariese, Dr. Tonu Reinot, Myungkoo Suh, Wook-Hyun Kim, Hsing-Mei Wu, Nick Milanovich for their help and keeping the research atmosphere a good one to work in. In Prof. Struve's group I would like to thank Dr. Herbert van Amerongen, Dr. Su Lin, Dr. Sergei Savikhin, and Chuck Smith for their assistance.

I am indebted to several organizations for their financial support. In particular I want to mention Ames Laboratory, Department of Chemistry, and Dow Chemicals.

Above all I am grateful to my parents, not only for their sacrificial assistance but also for their steady encouragement and unfalling love.

This work was performed at Ames Laboratory under Contract No. W-7405-Eng-82 with the U.S. Department of Energy. The United States goverment has assigned the DOE Report number IS-T1754 to this thesis.

APPENDIX A. A HOLE BURNING STUDY OF THE CP43 COMPLEX

I. Introduction

CP43 protein complex is one of the interior Chl *a* light-harvesting antenna protein complexes for Photosystem II (PSII) [1]. The inner antenna of PSII of higher plants consists of two chlorophyll-protein complexes denoted as CP43 and CP47 according to their apparent molecular weights. It is generally assumed that the inner antenna, both CP47 and CP43, accept the excitation energy from the light-harvesting complex (LHC) and transfer it further to the reaction center [1]. The CP43 antenna can be easily detached from the PSII reaction center by increasing the detergent (dodecyl maltoside) concentration to over 1% [2]. Detachment of CP43 can also be observed in the PSII particles after treatment with strong reductant dithionite at a concentration of 2 mg(mg Chl)$^{-1}$ [2]. It was not possible to detach the antenna CP47 under similar conditions. Therefore, it has been suggested that the CP43 antenna is less closely associated with the D1-D2-Cyt b_{559} reaction center than is CP47.

The absolute structure of CP43 is not known [1]. As in CP47, hydropathy plots of CP43 can be interpreted by six membrane-spanning helixes. Six helixes are connected by five hydrophilic loops. The total number of histidyl residues, the possible Chl *a* binding site, in CP43 is 12 [1]. There is a considerable debate in literature about the Chl *a* content in CP43 complex [1,3,4]. For example, de Vitry et al. suggested that both CP47 and CP43 bound 20-25 chlorophylls/ protein [3], while Barbato et al. [4] found 9-12 Chl *a* per CP47 and CP43 complexes.

CP43 and CP47 were previously thought to be only Chl *a* and β-carotene binding

proteins [1,5]. Photoprotective energy dissipation is one of the important functions of β-carotene, due to a lower triplet energy level than those of chlorophyll. Recently, xanthophyll lutein, which also functions as dissipating excess of excitation energy into heat, was found in CP43 and CP47 [5]. So the regulation of energy transfer to the reaction center could be one of the important functions for CP43 and CP47.

The low temperature (8K) absorption and emission spectra of CP43 were reported by Carbonera et al.[6]. The absorption maxima of CP43 complex are at 437, 668, 681 nm, while the fluorescence maximum is located at about 682nm [6]. Picorel et al. [7] showed that the Q_y absorption bands of CP43 at T=48 K could be resolved into four spectroscopic transitions of Chl *a* peaking at 682.3, 678.4, 671.5, and 661.4 nm. At 77 K fluorescence maximum was measured at ~685 nm [1]. At 8 K, ODMR spectra revealed two triplet states peaking at 683 and 668 nm, respectively [6]. The former (683 nm) was assigned as the lowest energy component of the antenna funnel in CP43 [6].

II. Results

A. Absorption Spectra

The absorption spectra of CP43 protein complex from two different preparations were obtained at low temperature (4.2 K). Figure 1 shows the low temperature absorption and its fourth derivative spectrum (4.2 K) of the first preparation denoted as CP43(I). The fourth derivative (dashed line) reveals one major band located at 682.8 nm associated with four additional higher energy bands located at 678.5, 672.2, 668.1, 664.7 nm, respectively.

In contrast to the pronounced ~683 nm absorption band revealed in the CP43(I) complex, the second preparation (CP43(II)) shows less intensity in that region, as illustrated in Figure 2a. Although the contribution from the ~683 nm band depends on

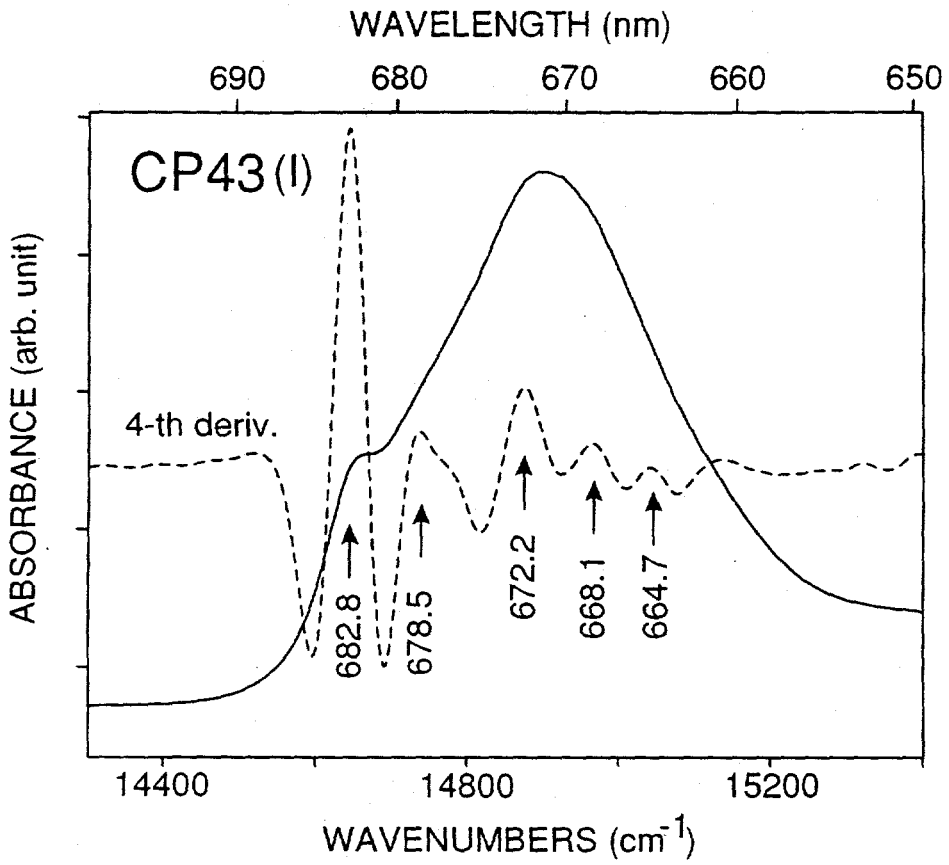

Figure 1. Absorption (Q_y-region) of CP43 (I) protein complex obtained at 4.2 K (solid line). Positions of the peaks revealed in fourth derivative (dashed line) are labeled.

preparation, the absorption spectra and their fourth derivatives are quite similar.

The difference between the above discussed preparations (i.e., CP43(I)-CP43(II)) is shown in Figure 3 (curve c) revealing the contribution of pigments absorbing at ~683 and 670 nm, respectively. In addition, the major absorption maximum at ~670 nm in CP43(I) (Figure 3a) is 2-3 nm blue shifted when compared with CP43(II) (Figure 3b).

B Persistent Hole Burned Spectra

Several nonphotochemical hole burned spectra obtained at various burn wavelengths at 4.2 K are shown as Figure 4 and 5 for CP43(I) and CP43(II), respectively. Persistent hole-burning spectra in Figure 4 were obtained with λ_B =675 nm (a), 670 nm (b), and 655 nm (c) respectively. The broad hole (FWHM~90 cm^{-1}) located at 682.8 nm is invariant to λ_B as indicated by solid arrows. Thus, these ~683 nm Chls serve as the lowest energy trap. An additional satellite hole located at ~670 nm can be identified in curve a, although the interference from an antihole make the observation of the ~670 nm satellite hole difficult. Vibronic holes are revealed when λ_B =655 nm is utilized. The numbers correspond to the vibrational frequencies in the excited state of Chl *a* absorbing in ~678 nm region. These low-frequency modes are compared in Table I with the data obtained from Chl *a* in PSI [8].

Two persistent hole burned spectra of CP43(II), shown in Figure 5, were obtained with λ_B =659.8 nm (curve a), 658.8 nm (curve b), respectively. Similar vibronic hole-burned spectra were obtained. Due to a small difference in excitation energy (~20 cm^{-1}) between curves a and b, all of the low energy fine features keep track of laser frequency and are blue-shifted about 20 cm^{-1} in curve b in comparison with curve a. The key observation is that the intensity of the invariant broad hole at ~683 nm is drastically reduced in CP43(II).

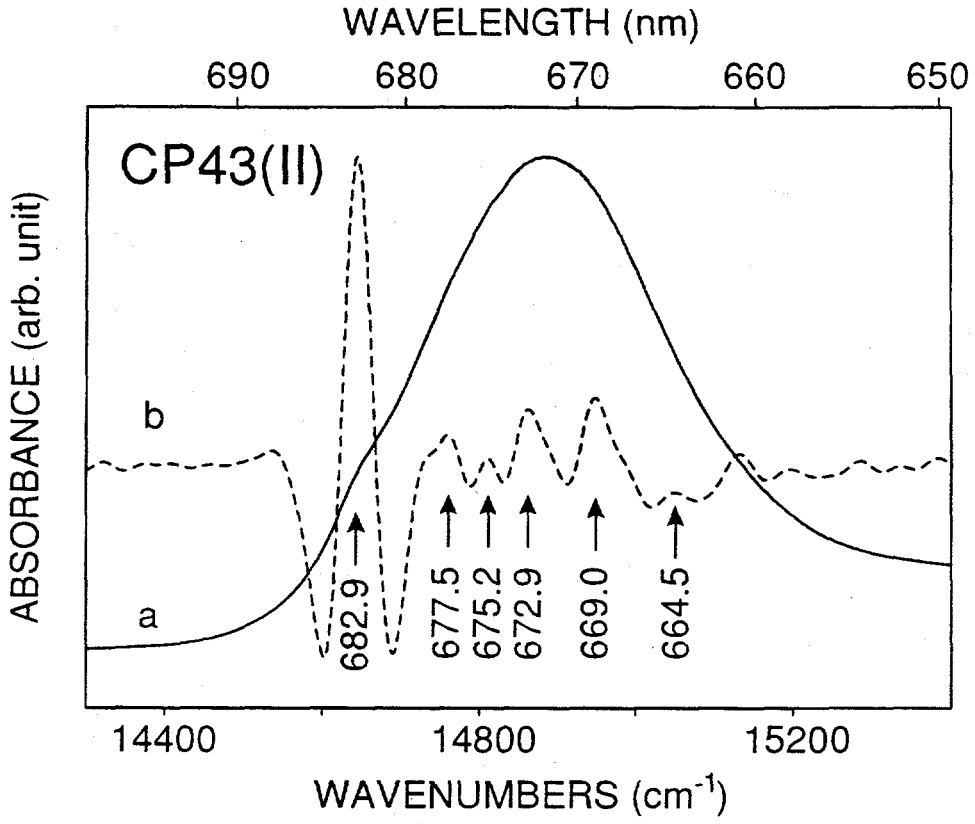

Figure 2. Absorption (Q_y-region) of CP43 (II) protein complex obtained at 4.2 K (solid line). Positions of the peaks revealed in fourth derivative (dashed line) are labeled.

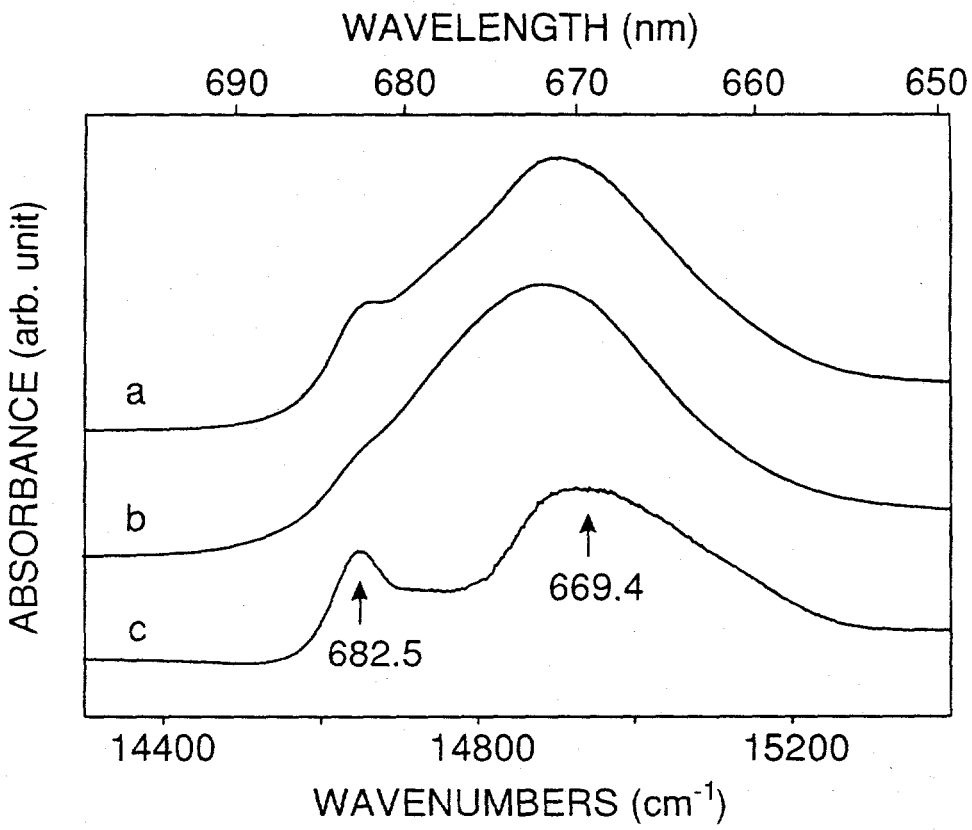

Figure 3. Low temperature (4.2 K) absorption (Q_y-region) of CP43 (I) (curve a) and CP43 (II) (curve b). The difference (curve c) between curve a and b reveals two maxima located at 682.5 and 669.4 nm, respectively.

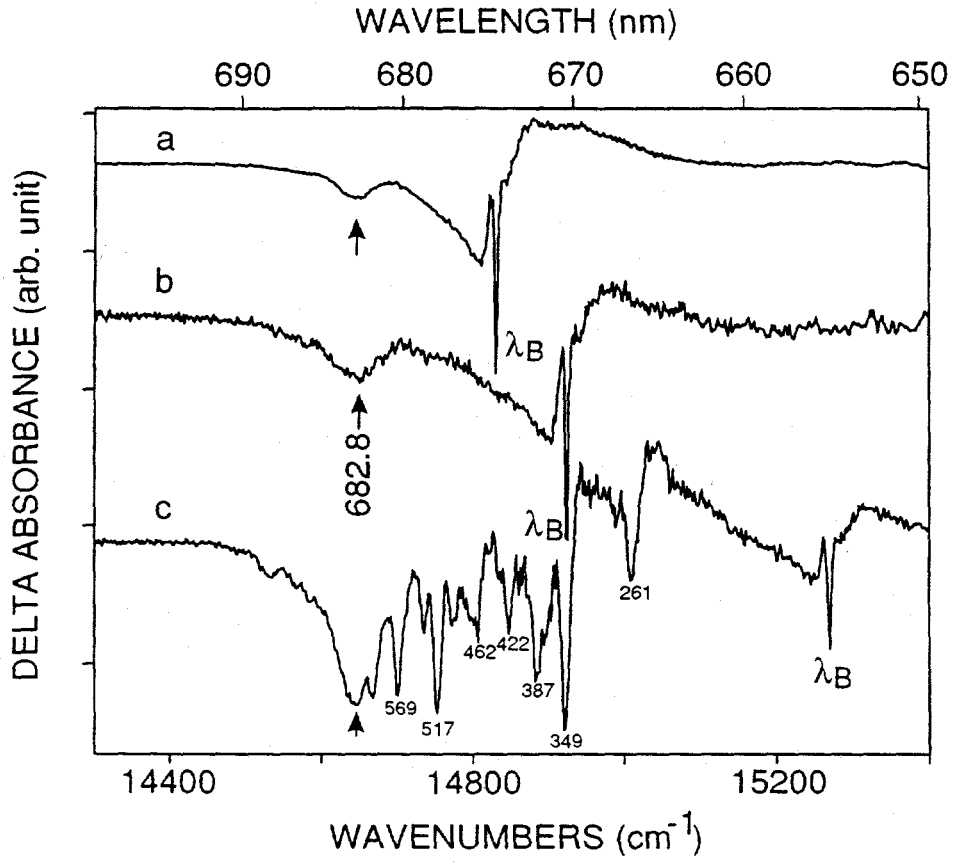

Figure 4. Persistent nonphotochemical hole burned spectra of CP43 (I) obtained at 4.2 K with λ_B= 675 nm (curve a), 670 nm (curve b), and 655 nm (curve c), respectively. The vibrational frequencies of vibronic holes are labeled in curve c.

Table 1. Vibrational frequency (cm^{-1}) obtained by nonphotochemical hole burning.

CP43	PSI
261	262
----	283
349	----
387	390
422	425
462	469
495	501
517	521
535	541
569	574
----	588

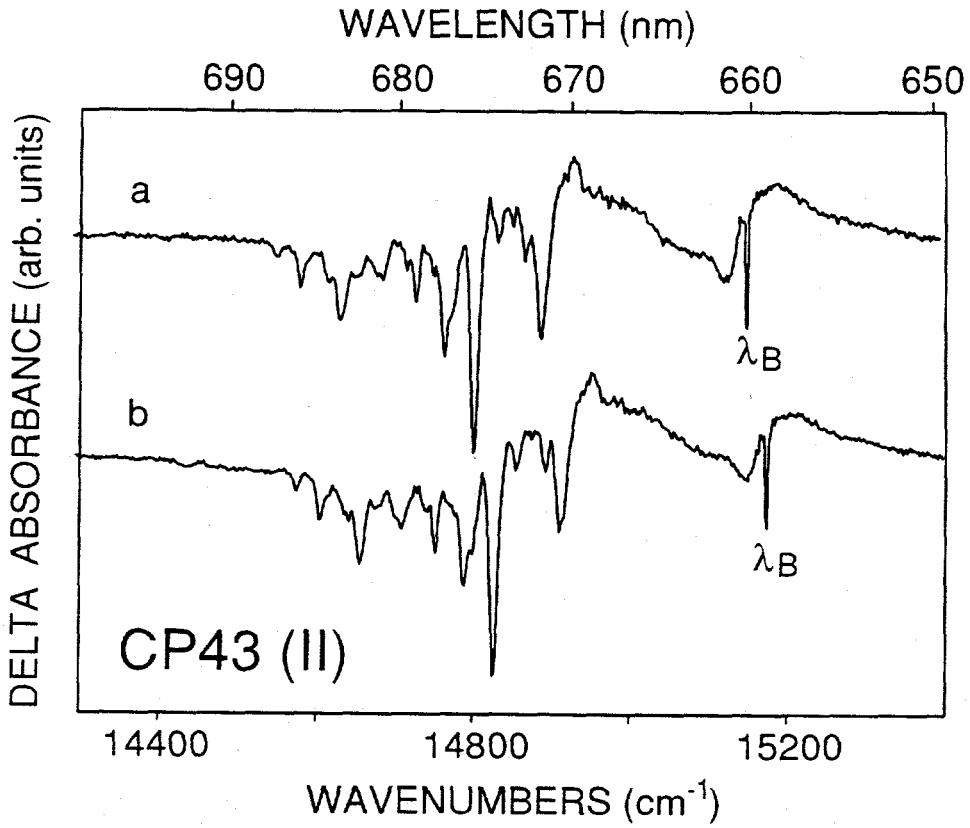

Figure 5. Persistent nonphotochemical hole burned spectra of CP43 (II) obtained at 4.2 K with λ_B= 660 nm (curve a) and 659 nm (curve b), respectively.

Hole burning data of CP43(I) obtained with burn wavelength of λ_B= 675, 680.5, and 682 nm are shown as Figure 6. Two shallow holes located at ~671 and ~678 nm are identified as indicated by dashed arrows. Interestingly, the position of these two satellite holes is invariant to λ_B (dashed arrows).

Hole burned spectra of CP43(II) are shown in Figure 7. Again two satellite holes located at ~671 and ~678 nm are also revealed in the antihole region. The observed cusp-like features just to the right of the ZPH are yielded by the interference between the real-phonon sideband hole and the anti-hole.

C Transient Hole Burned Spectra

The population-bottleneck hole burned spectra of CP43(I) (see Figure 8) revealed two broad features at ~683 nm and ~670 nm. As expected, the 683 nm band is greatly reduced in the population-bottleneck hole burned spectra of CP43(II) (data not shown). In curve a and b of Figure 8, the 683 nm hole feature exhibited abrupt termination at λ_B. It is possible that the 683 nm band is inhomogeneously broadened. The ~670 nm hole (curve c) has a much larger bandwidth than the 683 nm hole. It is interesting to note that the difference between CP43(I) and CP43(II) (shown in Figure 3c) also reveals a component at ~670 nm. This 670 nm band also exists in the population-bottleneck hole burned spectra of CP43(II) (data not shown).

III. Discussion

A. Absorption Spectra

The 4.2K absorption spectra, i.e., Figure 1 and 2, exhibit one band at ~683 nm associated with several partially resolved bands at a higher energy side. Interestingly, a 684 nm band with Γ_{inh} =110 cm^{-1} was recently found in CP47 and D1-D2-cyt b_{559} protein complexes. The question arises, do these two bands show similar hole burning

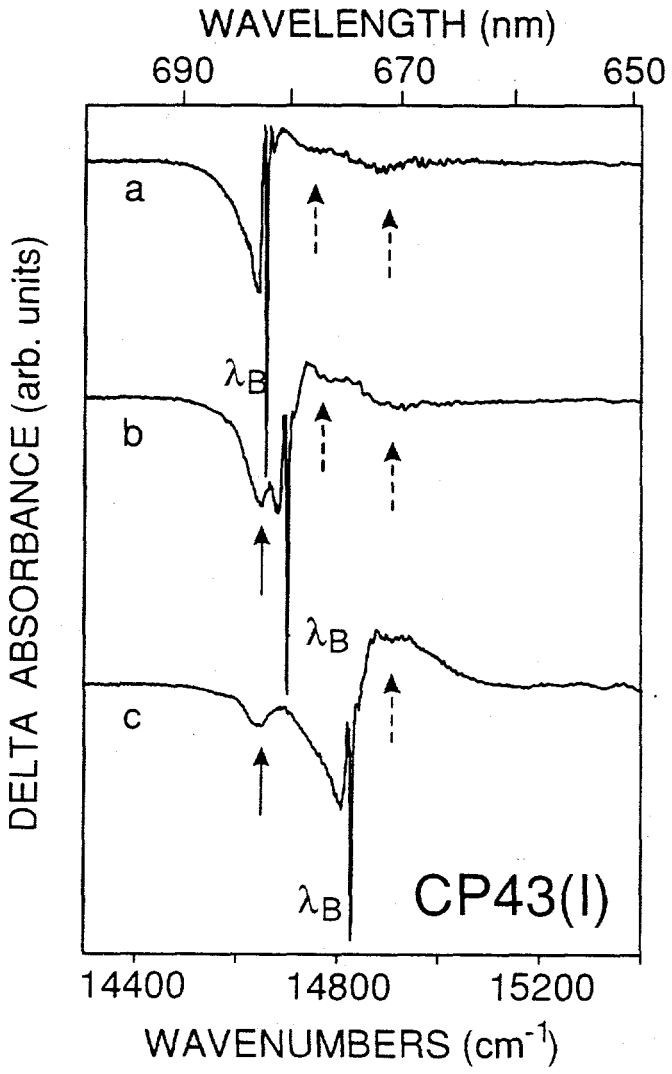

Figure 6. Persistent holes of CP43 (I) obtained with λ_B= 682 nm (curve a), 680 nm (curve b), and 675 nm (curve c), respectively. Satellite holes located at high energy side are indicated by dashed arrows.

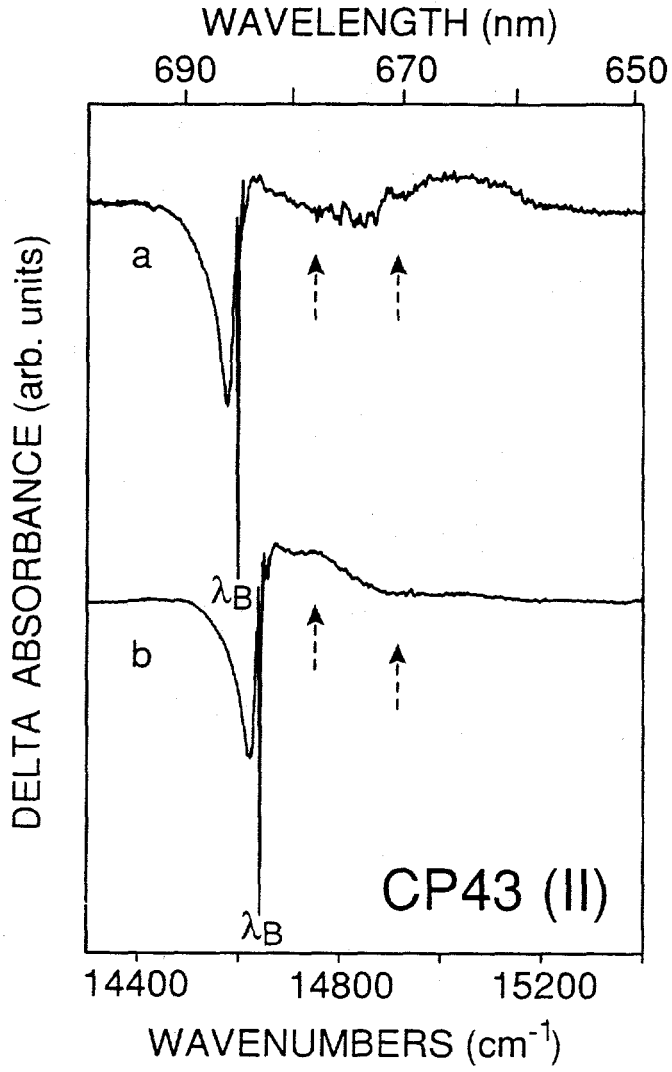

Figure 7. Persistent holes of CP43 (II) obtained with λ_B= 685 nm (curve a), and 682.5 nm (curve b), respectively. Satellite holes located at high energy side are indicated by dashed arrows.

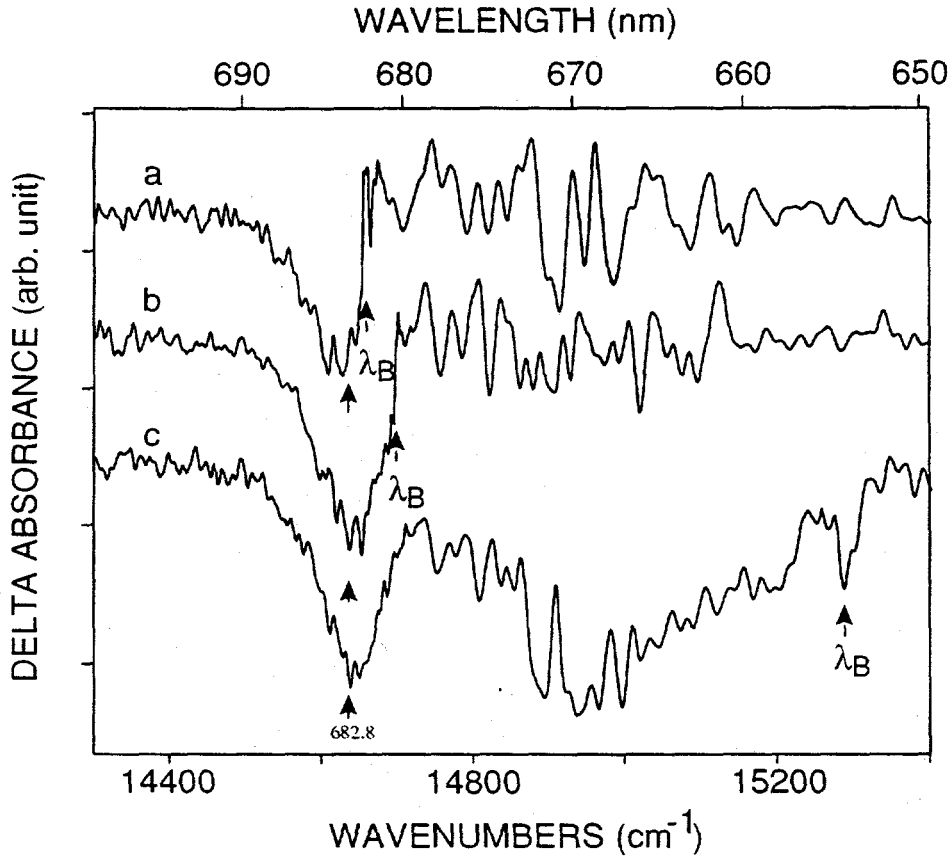

Figure 8. Low temperature (4.2 K) transient triplet bottleneck hole-burned spectra from CP43 (I) with λ_B =682 nm (curve a), 680 nm (curve b), and 655 nm (curve c), respectively.

patterns? This will be addressed below. The 670 nm broad feature revealed in the difference spectrum (Figure 3c) is also observed in transient hole spectra (two holes located at 670 and 683 nm, respectively). One should notice that these two transient holes (at 670 and 684 nm) are not connected, i.e., they originate from two different triplet bottlenecks (*vide infra*). We notice that ODMR experiments [6] also observed a ~670 nm band. It has been demonstrated that all preparations may contain some contribution from the dysfunctional Chls [8-10]. In contrast to the suggestion of disrupted Chl *a*, this band is assigned to an upper exciton band of a possible Chl *a* dimer or, simply showed an interaction with a different chlorophyll population absorbing at higher energy [6].

B. Persistent Hole Burned Spectra

The Stokes shift between the absorption and fluorescence origin bands is given by $2S\omega_m$, where ω_m is the mean phonon frequency. Persistent hole burned spectra indicated that a sharp zero-phonon hole can be observed at λ_B =682 nm (see Figure 6 and 7). Carbonera et al. [2] also reported ~682 nm to be the fluorescence maximum at 8K. All the observations given above indicate that the linear electron-phonon coupling of the 683 nm state is weak (S<1).

We note that the spectra of both Figure 6 and 7 show that hole burning of the low energy bands elicits weak responses from the higher energy absorption bands at ~671 and ~678 nm. It is interesting to note that these weak responses do not drastically diminish in CP43(II), which has much less 683 nm band, as revealed in Figure 5. This observation strongly suggests the satellite hole at 683 nm is not excitonically correlated with the higher energy holes at ~671 and ~678 nm. That is, the 683 nm band does not belong to a part of the CP43 exciton-interacting pigments. It is possible that another lower energy state, which is revealed in the low energy tail of CP43(II) (see Figure 2), serves as a shuttle state

for energy downward transfer between the higher energy state and the 683 nm band. In summary, based on the satellite hole structure observed in Figure 6 and 7, two states at 671 and 678 nm are identified as being excitonically correlated with the shuttle state which is located at the low energy side of CP43 absorption spectrum. The constant fluence action spectrum may provide further confirmation. The 683 nm hole, which can be further washed out, may not be one of the exciton states in CP43 protein complex. Similar behavior was revealed in the CP47 protein complex.

The pseudo-vibronic structures revealed with high energy excitation (Figure 4 and 5) provide the evidence for the existence of some disrupted Chl *a* in both CP43(I) and CP43(II). That is, the high resolution ZPH measurements may not accurately reflect the dynamics of fully functional energy transfer time in both CP43(I) and CP43(II).

C. Transient Hole-Burning Spectra

The broad feature located at 670 nm appears in both the difference absorption spectrum (Figure 3c) and the population bottleneck hole burned spectra (Figure 8c). The key observation is that this 670 nm hole is diminished with lower excitation energy (Figure 8a and b). This observation invalidates the suggestion of Carbonera et al. that the 670 nm band may be due to an upper exciton band. Van Kan el al. [11] also reported an intense feature at 670 nm in the population bottleneck hole burned spectra in the CP47 protein complex. They concluded that it is most likely due to non-native Chl molecules produced by the isolation and/or sample handling procedures.

The 683 nm feature exhibited abrupt termination at λ_B (shown in Fig.8a and b). This result indicates the 683 nm band is inhomogeneously broadened. Similar behavior was reported for the 684 nm band in CP47. See Chapter 4 for more explainations.

References

1. Bricker, T.M. *Photosyn. Res.* 1990, 24, 1.

2. Giardi, M.T. *Planta* 1993, 190, 107.

3. De Vitry, C.; Wollmann, F-A.; Delepelaire, P. *Biochim. Biophys. Acta* 1984, 767, 415.

4. Barbato, R.E.; Rigoni, F.; Giardi, M.T.; Giacometti, G.M. *FEBS Lett.* 1989, 251, 147

5. Bassi, R.; Pineau, B.; Dainese, P.; Marquardt, J. *Eur. J. Biochem.* 1993, 212, 297.

6. Carbonera, D.; Giacometti, G.; Agostini, G.; Angerhofer, A.; Aust, V. *Chemiacl Physics Letters* 1992, 194, 275.

7. Picorel, R. private communication

8. Gillie, J.K.; Small, G.J.; Golbeck, J.H. *J. Phys. Chem.* 1989, 93, 1620

9. Chang,H-C.; Jankowiak,R.; Yocum,C.F.; Picorel,R.; Alfonso,M.; Seibert,M.; Small,G.J. *J. Phys. Chem.* 1994, 98, 7717.

10. Chang,H-C.; Jankowiak,R.; Reddy,N.R.S.; Yocum,C.F.; Picorel,R.; Seibert,M.; Small,G.J. *J. Phys. Chem.* 1994, 98, 7725

11. Van Kan, P.J.M.; Groot, M.L.; van Stokkum, I.H.M.; Kwa, S.L.S.; van Grondelle, R.; and Dekker, J.P. in *Research in Photosynthesis*, Vol.1; Murata, N., Ed.; Kluwer: Netherlands, 1992, 271

APPENDIX B: COMPARISON OF THE ABSORPTION SPECTRA OF THE PHOTOSYSTEM II D1-D2-CYT B_{559} REACTION CENTER FROM TWO DIFFERENT PREPARATIONS

It is informative to examine the difference between absorption spectrum of D1-D2-cyt b_{559} protein complexes prepared by two groups, i.e. Seibert (socalled 4 Chl *a* preparation) and Dekker, respectively. In earlier work [1], samples prepared by the procedures of McTarish et and Dekker et al. were studied utilizing hole burning technique. It was shown that the charge separation and energy transfer dynamics of the two preparations are very similar. Recently it was found that the relative Chl *a* content of the sample can be determined by normalizing the intensities of the Q_X-band of Pheo *a* at 543 nm [2,3]. It is assumed that the absorption from Chl *a* and carotenoid only contribute to the broad background absorption which underlies the sharp Pheo *a* band at 543 nm. Low temperature (4.2 K) absorption spectra of preparations from Seibert (dashed line) and Dekker (solid line) are normalized to the same intensity of the Q_X-band of Pheo *a* as shown in Figure 1. The extent to which the Pheo *a* Q_X-band is resolved is illustrated by the inset spectra of Figure 1. A straight line obtained by the subtraction of Q_X-band of Pheo *a* ensures that the normalization procedure is performed correctly (see inset). The normalized absorption spectra at the Q_Y-region from Seibert's (curve a) and Dekker's (curve b) preparations are shown in Figure 2. Comparison of the two indicates that Dekker's preparation has a higher Chl *a* content. Assuming that the Dekker preparation has ~6.4 Chl *a*/ 2 Pheo, as recently measured by HPLC method [4], the integration of the absorption spectrum of the Seibert preparation estimates the number of Chl *a*/ 2 Pheo as 5.3. Subtraction of spectra a and b, i.e. curve c, reveals that Dekker's preparation has less

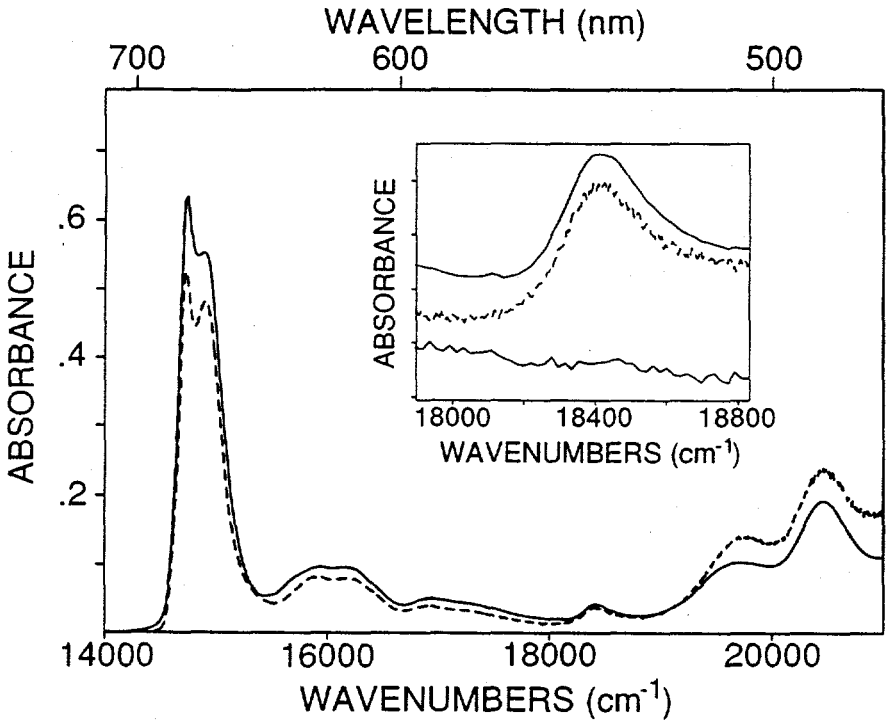

Figure 1 Low temperature (4.2 K) absorption spectra of D1-D2-cyt b_{559} protein complexes prepared by Seibert (dashed line) and Dekker (solid line), respectively. The spectra were normalized to the same intensity of the Q_X band of Pheo *a* (see inset). The difference between these two preparations in Q_X region is shown as the lower trace (see inset also).

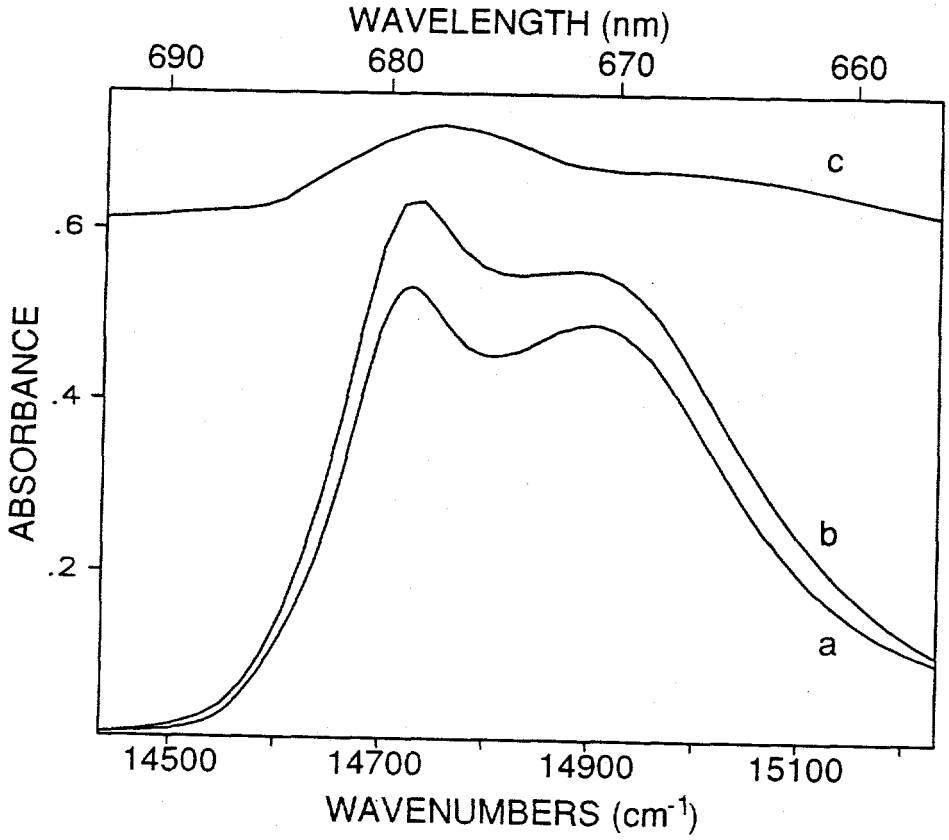

Figure 2. Absorption (Q_y-region) of D1-D2-cyt b559 complexes prepared by Seibert (curve a) and Dekker (curve b), respectively. Curve c corresponds to the difference between the absorption spectra of Dekker's and Seibert's preparations.

contribution from dysfunctional Chl *a* absorbing at ~670 nm, but may contain some contribution from the 684 nm band and/or CP47-D1-D2-cyt b_{559}. Chang et al. [3] discussed the complications associated with proper stoichiometry assignment when the preparation is contaminated with CP47 and/or dysfunctional Chl *a*. Considerable evidence exists [5] which indicates that the Chl *a*/ Pheo *a* ratio depends on the isolation procedure and other factors. Holzwarth's group studied the picosecond fluorescence kinetics of long-term (samples from Shuvalov) [6] and short-term (from Dekker) [7] Triton-exposed RC particles. An ultrashort component of 1-6 ps, which has been resolved in samples from Shuvalov, was not resolved in Dekker's samples. The absence of the ultrashort component, assigned to the primary charge separation time, was attributed to the larger chlorophyll content of Dekker's preparation [7]. It is known that the maximum position of P680 transient holes is dependent on the purity of the RC preparations [3,8]. One should notice that the maximum position of the P680 hole of Dekker's preparation [9] lies between that of the 4 and 6 Chl *a*/ RC preparations [3].

References

1. Tang, D.; Jankowiak, R.; Seibert, M.; Yocum, C.F.; Small, G.J. *J. Phys. Chem.* 1990, 94, 6519

2. Chang, H.-C.; Jankowiak, R.; Yocum, C.F.; Picorel, R.; Alfonso, M.; Seibert, M.; Small, G.J. *J. Phys. Chem.* 1994, 98, 7717

3. Chang, H.-C.; Jankowiak, R.; Reddy, N.R.S.; Yocum, C.F.; Picorel, R.; Seibert, M.; Small, G.J. *J. Phys. Chem.* 1994, 98, 7725

4. Dekker, J.P. Private communication

5. Seibert, M. in *The Photosynthetic Reaction Center*; Vol.I; Deisenhofer, J., Norris, J., Eds.; Academic Press: New York, 1993, p.319

6. Roelofs, T.A.; Gilbert, M.; Shuvalov, V.A.; Holzwarth, A.R. *Biochim. Biophys. Acta* 1991, 1060, 237

7. Roelofs, T.A.; Kwa, S.L.S.; van Grondelle, R.; Dekker, J.P.; Holzwarth, A.R. *Biochim. Biophys. Acta* 1993, 1143, 147

8. Jankowiak, R.; Small, G.J. in *The Photosynthetic Reaction Center*; Vol.II; Deisenhofer, J., Norris, J., Eds.; Academic Press: New York, 1993, p.133

9. Kwa, S.L.S.; Eijckelhoff, C.; van Grondelle, R.; Dekker, J.P. *J. Phys. Chem.* 1994, 98, 7702